Can Stellar-mass Black Hole Growth Disrupt Disks of Active Galactic Nuclei? The Role of Mechanical Feedback

Hiromichi Tagawa[1], Shigeo S. Kimura[1,2] , Zoltán Haiman[3] , Rosalba Perna[4,5] , Hidekazu Tanaka[1] , and Imre Bartos[6]
[1] Astronomical Institute, Graduate School of Science, Tohoku University, Aoba, Sendai 980-8578, Japan; htagawa@astr.tohoku.ac.jp
[2] Frontier Research Institute for Interdisciplinary Sciences, Tohoku University, Sendai 980-8578, Japan
[3] Department of Astronomy, Columbia University, 550 W. 120th St., New York, NY 10027, USA
[4] Department of Physics and Astronomy, Stony Brook University, Stony Brook, NY 11794-3800, USA
[5] Center for Computational Astrophysics, Flatiron Institute, New York, NY 10010, USA
[6] Department of Physics, University of Florida, PO Box 118440, Gainesville, FL 32611, USA
Received 2021 November 7; revised 2021 December 19; accepted 2021 December 20; published 2022 March 3

Abstract

Stellar-mass BHs (sBHs) are predicted to be embedded in active galactic nucleus (AGN) disks owing to gravitational drag and in situ star formation. However, we find that, due to a high gas density in an AGN disk environment, compact objects may rapidly grow to intermediate-mass BHs and deplete matter from the AGN disk unless accretion is suppressed by some feedback process(es). These consequences are inconsistent with AGN observations and the dynamics of the Galactic center. Here we consider mechanical feedback mechanisms for the reduction of gas accretion. Rapidly accreting sBHs launch winds and/or jets via the Blandford–Znajek mechanism, which produce high-pressure shocks and cocoons. Such a shock and cocoon can spread laterally in the plane of the disk, eject the outer regions of a circum-sBH disk (CsBD), and puncture a hole in the AGN disk with horizontal size comparable to the disk scale height. Since the depletion timescale of the bound CsBD is much shorter than the resupply timescale of gas to the sBH, the time-averaged accretion rate onto sBHs is reduced by this process by a factor of ~ 10–100. This feedback mechanism can therefore help alleviate the sBH overgrowth and AGN disk depletion problems. On the other hand, we find that cocoons of jets can unbind a large fraction of the gas accreting in the disks of less massive supermassive BHs (SMBHs), which may help explain the dearth of high-Eddington-ratio AGNs with SMBH mass $\lesssim 10^5 \, M_\odot$.

Unified Astronomy Thesaurus concepts: Stellar mass black holes (1611); Active galactic nuclei (16); Accretion (14); Black hole physics (159); Galactic center (565); Jets (870)

1. Introduction

Massive galaxies are observed to have supermassive black holes (SMBHs) in their centers (e.g., Kormendy & Ho 2013, for a review). It is well established that SMBHs have mainly grown via gas accretion from the disks of active galactic nuclei (AGNs) at least at redshifts $z \lesssim 5$ (e.g., Yu & Tremaine 2002). Several studies have suggested that densely populated stars and compact objects, including stellar-mass BHs (sBHs) in nuclear star clusters (e.g., Miralda-Escude & Gould 2000; Lu et al. 2013), are captured and embedded in AGN disks (Ostriker 1983; Syer et al. 1991) and that stars actively form in the outer regions of AGN disks (Goodman 2003; Thompson et al. 2005; Nayakshin et al. 2007). There are several observations supporting this picture (Artymowicz et al. 1993; Levin & Beloborodov 2003; Tagawa et al. 2020b). Additionally, AGN disks are promising environments to explain the characteristic properties of some unexpected gravitational wave events discovered by LIGO/Virgo, such as the massive binary merger event GW190521 (e.g., Abbott et al. 2020; Samsing et al. 2020; Tagawa et al. 2021b, 2021c) and its hypothesized electromagnetic counterpart (Graham et al. 2020). However, if sBHs in AGN disks accrete without any feedback (e.g., Lubow et al. 1999; Levin & Beloborodov 2003; Levin 2007; Tanigawa & Tanaka 2016; Dittmann et al. 2021), sBHs rapidly grow to intermediate-mass BHs (IMBHs) or SMBHs within the lifetime of

AGNs (Goodman & Tan 2004) and deplete most accreting gas, which contradicts quasar observations (e.g., Yu & Tremaine 2002) and the dynamics of the Galactic center (Naoz et al. 2020; Gravity Collaboration et al. 2020).

There are several feedback processes that may suppress rapid accretion. One is mechanical feedback by winds launched from the inner region of a rapidly accreting circum-sBH disk (CsBD; e.g., Jiang et al. 2014; Sadowski et al. 2015; Regan et al. 2019). However, the wind expected under conditions of super-Eddington accretion is predicted to be launched anisotropically (e.g., Jiao et al. 2015; Kitaki et al. 2021), and the gas inflow outside the wind opening angle is only modestly suppressed as long as the wind is not decelerated in a shock (Takeo et al. 2020). If most of the inflowing gas is ejected as the wind (e.g., Sadowski et al. 2015), the feedback would be stronger, and the growth of sBHs can be suppressed. On the other hand, the outflow rate for super-Eddington accretion is suggested to be modest when the trapping radius is much smaller than the circularization radius (Kitaki et al. 2021), which is the case for accretion onto sBHs in AGN disks (e.g., Tanigawa et al. 2012). Most of the previous studies have not investigated the wind feedback for the situations in which the wind is thermalized. Although Kimura et al. (2021a) and Wang et al. (2021a, 2021b) examined the evolution of bubbles around sBHs due to the winds, they did not estimate the amount of the CsBD and surrounding gas ejected by the wind bubbles and its global importance for the AGN.

Another is radiation-pressure-driven ejection (e.g., Inayoshi et al. 2016; Toyouchi et al. 2019). An optically and geometrically thick inner CsBD is formed for a super-Eddington accretion flow,

the radiation from the inner regions escapes perpendicular to the disk, and gas inflow along the disk plane is not significantly suppressed (Sugimura et al. 2017; Toyouchi et al. 2021). Additionally, in dense environments like AGN disks, rapid accretion is not suppressed by radiation even if it is isotropic (Inayoshi et al. 2016). Thus, to solve the overgrowth and depletion problems, additional feedback processes are likely required.

In this paper we focus on a regulation process for accretion, mediated by the evolution of a cocoon generated around a jet launched by an accreting and rotating sBH due to the Blandford–Znajek (BZ) mechanism (Blandford & Znajek 1977). In this process, the cocoon can interact with and eject the CsBD as it spreads laterally toward the disk plane from the jet head, due to its high pressure coupled with local density gradients in the AGN disk near the sBH. Such a feedback process is often called a jet feedback mechanism (JFM) and plays important roles in several contexts (e.g., Soker 2016, for a review), such as galaxy clusters (e.g., McNamara & Nulsen 2012), galaxy formation (e.g., Fabian 2012), planetary nebulae (e.g., Balick & Frank 2002), common envelope evolution (e.g., Soker 2014), and young stellar objects (e.g., Frank et al. 2014, pp. 451–474). Here we apply the JFM to the system of accreting sBHs in AGN disks. The JFM in the AGN disk is similar to that in common envelope evolution (e.g., Moreno Méndez et al. 2017; López-Cámara et al. 2019; Grichener et al. 2021; Hillel et al. 2021), while there are many differences (the density and geometry of surrounding gas, the angular momentum of the CsBD, and the jet luminosity). Particularly, we found that the JFM for accretion in the AGN disk can eject the outer regions of the CsBD, which has not appeared in the other contexts. Similarly, a wind launched from the CsBD can eject the outer CsBD through strong shocks. However, we find that the CsBD is typically more efficiently ejected by the JFM, due to its higher pressure compared to the wind shock. We therefore focus on the JFM in the main text and comment on the relative importance of wind feedback in Appendix B.3. We find that this regulation process can reduce the accretion rate by a factor of $\sim$10–100, depending on the model parameters. We use the cylindrical coordinates (z, r) and (Z, R), with $z = r = 0$ and $Z = R = 0$ representing the positions of the sBH and the SMBH, respectively. The $Z = 0$ plane is set to the AGN plane, and the z-axis represents the direction of the jet propagation. Unless stated otherwise, we assume below that the z-axis is aligned with the Z-axis.

2. Rapid Accretion Problems

We first outline the key issue related to the evolution of compact objects in AGN disks, which is a rapid growth of compact objects (e.g., Goodman & Tan 2004; see also Cantiello et al. 2021; Jermyn et al. 2021, for stars). We estimate the growth rate of sBHs in an AGN disk without feedback as follows. For an sBH embedded in an AGN disk, the Bondi–Hoyle–Lyttleton radius ($r_{\rm BHL}$) usually exceeds the scale height of the AGN disk ($H_{\rm AGN}$) and the Hill radius ($r_{\rm Hill}$). Due to the limitation of capture regions by the shear motion and the vertical height of the AGN disk, the capture rate of gas by the sBH is given by

$$
\begin{aligned}
\dot{M}_{\rm cap} &= f_c \, r_w r_h \rho_{\rm AGN} (c_{s,\rm AGN}^2 + v_{\rm sBH}^2 + v_{\rm sh}^2)^{1/2} \\
&\simeq 3 \times 10^{-4} \, M_\odot \, {\rm yr}^{-1} \left(\frac{f_c}{10}\right) \left(\frac{H_{\rm AGN}}{0.003 \, {\rm pc}}\right) \left(\frac{R_{\rm sBH}}{1 \, {\rm pc}}\right)^{1/2} \\
&\quad \left(\frac{\rho_{\rm AGN}}{4 \times 10^{-17} \, {\rm g \, cm}^{-3}}\right) \left(\frac{M_{\rm sBH}}{10 \, M_\odot}\right)^{2/3} \left(\frac{M_{\rm SMBH}}{10^6 \, M_\odot}\right)^{-1/6}
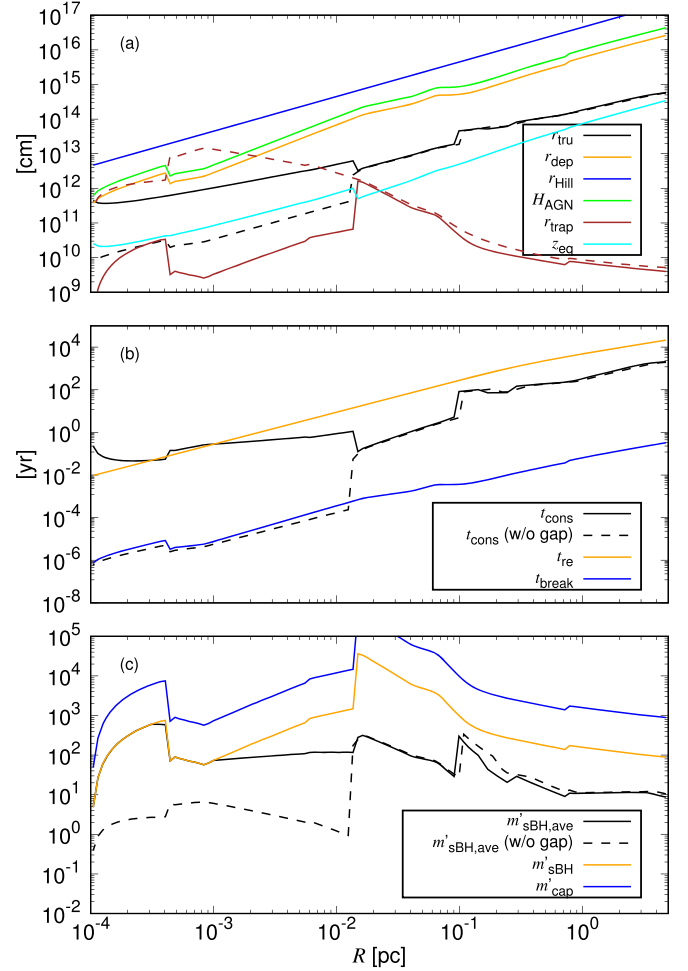\end{aligned}
\tag{1}
$$

Figure 1. Several model quantities as a function of R for the fiducial model (Section 3.2 and Table 1). (a) The truncation radius (black), depletion radius (orange), Hill radius (blue), AGN scale height (green), photon trapping radius (brown), and wind equilibrium height (cyan). (b) The timescales for CsBD gas consumption (black), resupply (orange), and jet breakout (blue). (c) The average accretion rate with the JFM (black), the accretion rate (orange), and the capture rate (blue) in units of the Eddington rate. In the case with dashed lines, a gap is assumed not to form in an AGN disk.

(e.g., Tanigawa & Tanaka 2016; Stone et al. 2017; Rosenthal et al. 2020), where $\rho_{\rm AGN}$ is the gas density and $c_{s,\rm AGN}$ is the sound speed of the AGN disk at the position of the sBH ($R_{\rm sBH}$), $v_{\rm sBH}$ is the velocity of the sBH with respect to the local motion of the AGN disk, $v_{\rm sh} = r_w (GM_{\rm SMBH}/R_{\rm sBH}^3)^{1/2}$ is the shear velocity at the capture radius $r_w = \min(r_{\rm BHL}, r_{\rm Hill})$, $r_h = \min(r_w, H_{\rm AGN})$ is the capture height, G is the gravitational constant, $M_{\rm SMBH}$ is the mass of the SMBH at the center of the AGN disk, and f_c is a normalization constant. We adopt $f_c = 10$ as found by Tanigawa & Watanabe (2002). In the second equality of Equation (1), we assume $v_{\rm sBH} < c_{s,\rm AGN} < v_{\rm sh}$ and $H_{\rm AGN} < r_{\rm Hill} < r_{\rm BHL}$. Figure 1 shows various variables as a function of R, and as can be seen in panel (a) of this figure, this assumption is satisfied in the disk model adopted in this paper. On the right-hand side of Equation (1) (and for the equations and figures below), the fiducial values for the model parameters (Section 3.2, Table 1) are adopted. The density and scale height of the AGN disk are derived from the model in Thompson et al. (2005) as constructed in Tagawa et al. (2020b). The accretion rate in units of the Eddington rate ($\dot{M}_{\rm Edd}(M)$ for the mass M)

Table 1
Fiducial Values of Our Model Parameters

Parameter	Fiducial Value
Radial distance of the sBH from the SMBH	$R_{\rm sBH} = 1$ pc
Jet energy conversion efficiency	$\eta_{lj} = 0.5$
Initial mass of the sBH	$M_{\rm sBH,ini} = 10\,M_\odot$
Mass of the SMBH	$M_{\rm SMBH} = 10^6\,M_\odot$
Gas inflow rate from the outer boundary of the AGN disk in units of the Eddington rate for $M_{\rm SMBH}$	$\dot{m}_{\rm SMBH} = 0.1$
Outer boundary of the AGN disk	$R_{\rm out} = 5$ pc
Angular momentum transfer parameter in the outer regions of the AGN disk	$m_{\rm AM} = 0.15$
Viscous parameter of the AGN disk	$\alpha_{\rm AGN} = 0.1$
Ratio of the sBH accretion rate to the gas capture rate	$f_{\rm acc} = 0.1$
Opening angle at the base of the jet	$\theta_0 = 0.2$
Radiative efficiency	$\eta_{\rm rad} = 0.1$
Viscous parameter of the CsBD	$\alpha_{\rm CsBD} = 0.3$
Ratio of the outer radius of the CsBD to the Hill radius	$f_{\rm circ} = 0.1$

with the conversion efficiency to radiation of $\eta_{\rm rad} = 0.1$ is

$$
\dot{m}_{\rm cap} = \dot{M}_{\rm cap}/\dot{M}_{\rm Edd}(M_{\rm sBH})
$$

$$
\simeq 2 \times 10^3 \left(\frac{f_c}{10}\right)\left(\frac{\eta_{\rm rad}}{0.1}\right)\left(\frac{R_{\rm sBH}}{1\,{\rm pc}}\right)^{1/2}
$$

$$
\left(\frac{H_{\rm AGN}}{0.003\,{\rm pc}}\right)\left(\frac{M_{\rm sBH}}{10\,M_\odot}\right)^{-1/3}\left(\frac{M_{\rm SMBH}}{10^6\,M_\odot}\right)^{-1/6}
$$

$$
\left(\frac{\rho_{\rm AGN}}{4 \times 10^{-17}\,{\rm g\,cm^{-3}}}\right) \tag{2}
$$

(blue line in Figure 1(c)). Also, sBHs are assumed to radially migrate in an AGN disk following the formulae developed for migration of planets in a protoplanetary disk (see Appendix A.4).

Figure 2 shows the evolution of the sBH mass ($M_{\rm sBH}$), as well as the time (t) from the beginning of the AGN phase for the sBH to grow to $M_{\rm sBH}$, as a function of $R_{\rm sBH}$ for several combinations of values for $M_{\rm SMBH}$, $R_{\rm ini}$, and $\dot{m}_{\rm SMBH}$ (see Appendix A.3 for equations), where $\dot{m}_{\rm SMBH} = \dot{M}_{\rm SMBH}/\dot{M}_{\rm Edd}(M_{\rm SMBH})$ is the gas inflow rate to the AGN disk in units of the Eddington rate for $M_{\rm SMBH}$.

Based on the sBH growth rate, we highlight two problems for the evolution of compact objects in AGN disks.

(i) *Depletion problem.* The number of captured sBHs ($N_{\rm sBH,AGN}$) can be estimated to be $N_{\rm AGN,sBH} \sim 60\text{--}1000(\dot{m}_{\rm Edd}/0.1)^{1/2}$ (Tagawa et al. 2020b, 2021c). This value is roughly consistent with the number of low-mass X-ray binaries in the Galactic center region (Hailey et al. 2018; Tagawa et al. 2020b; Mori et al. 2021) and the rates for some fraction of sBH mergers detected by LIGO-Virgo (e.g., GW190521) originating in AGNs (Tagawa et al. 2021c). By roughly assuming

$$
N_{\rm AGN,sBH} \sim 300\left(\frac{\dot{m}_{\rm SMBH}}{0.1}\right)^{1/2} \tag{3}
$$

and the mass of an sBH at the end of the AGN phase ($t_{\rm AGN} \sim 10\text{--}100$ Myr, e.g., Marconi et al. 2004; Greene & Ho 2007) to be

$$
M_{\rm sBH,fin} \sim 10^3\,M_\odot\left(\frac{M_{\rm SMBH}}{10^6\,M_\odot}\right)\left(\frac{\dot{m}_{\rm SMBH}}{0.1}\right)^{1/2} \tag{4}
$$

(from Figure 2), the gas in the AGN disk is depleted by the population of sBHs embedded in it at a rate

$$
\dot{M}_{\rm sBH,tot} \sim N_{\rm AGN,sBH}M_{\rm sBH,fin}/t_{\rm AGN}
$$

$$
\sim 3 \times 10^{-2} - 3 \times 10^{-3}\,M_\odot\,{\rm yr^{-1}}\left(\frac{M_{\rm SMBH}}{10^6\,M_\odot}\right)\left(\frac{\dot{m}_{\rm SMBH}}{0.1}\right). \tag{5}
$$

This exceeds the inflow rate of the AGN disk,

$$
\dot{M}_{\rm SMBH,in} \simeq 2 \times 10^{-3}\,M_\odot\,{\rm yr^{-1}}\left(\frac{M_{\rm SMBH}}{10^6\,M_\odot}\right)\left(\frac{\dot{m}_{\rm SMBH}}{0.1}\right), \tag{6}
$$

implying that the gas inflow can be depleted by sBHs if there is no feedback. This is the case irrespective of the SMBH mass and the gas inflow rate, as shown in Figure 3, which compares the depletion rate by sBHs and the inflow rate in the AGN disk. In this case, the growth of SMBHs may be dominated by the accretion of sBHs. This is in contradiction with Soltan's argument in which massive SMBHs have grown mainly via gas accretion during luminous AGN phases (e.g., Yu & Tremaine 2002). We should note that this conclusion depends on $N_{\rm sBH,AGN}$, which cannot be well constrained owing to uncertainties in the size of the AGN disk (e.g., Burtscher et al. 2013; Stalevski et al. 2019), in the stellar initial mass function in galactic centers (Lu et al. 2013), and in the anisotropy of the velocity dispersion of sBHs caused by vector resonant relaxation (Szolgyen & Kocsis 2018).

(ii) *Overgrowth problem.* In the Galactic center, a third object with a mass of $\gtrsim 100\,M_\odot$ is prohibited within $R_{\rm sBH} \sim 10^{-3}\text{--}10^{-2}$ pc from Sgr A* (Naoz et al. 2020; Gravity Collaboration et al. 2020). If sBHs efficiently grew in a possible AGN disk around Sgr A* in ~ 10 Myr (Su et al. 2010), there would not be enough time for the grown sBHs ($M_{\rm sBH} \sim 10^2\text{--}10^3\,M_\odot$) to migrate and merge to Sgr A* in the quiescent phase (e.g., Merritt 2010). Hence, the evolution of sBHs without feedback (Figure 2) is likely inconsistent with observations of stellar orbital dynamics in the Galactic center.

To resolve these possible problems and contradictions, there ought to be some mechanism to regulate the growth of sBHs in AGN disks. While there are established feedback processes regulating gas accretion onto sBHs, it is unclear whether these can sufficiently suppress the time-averaged accretion rate in these systems (Appendix B.1), motivating the present study of a different mechanism.

3. Regulation of Gas Accretion

3.1. Overview of the Regulation Process

We begin with an overview of our model, in which gas accretion onto an sBH in an AGN disk is regulated by a cocoon produced around a jet. A schematic picture of the regulation is shown in Figure 4. We propose that an accreting sBH embedded in an AGN disk experiences the following episodes:

1. The jet evacuates a large hollow region ($r_{\rm dep} \sim 5 \times 10^{15}$ cm; Equation (12)) very quickly ($t_{\rm break} \sim 0.04$ yr; Equation (13)).
2. Inside this hollow region, the outer part of CsBD is blown away, and only a small inner portion of the CsBD survives (inside $r_{\rm tru} \sim 2 \times 10^{14}$ cm; Equation (9)).
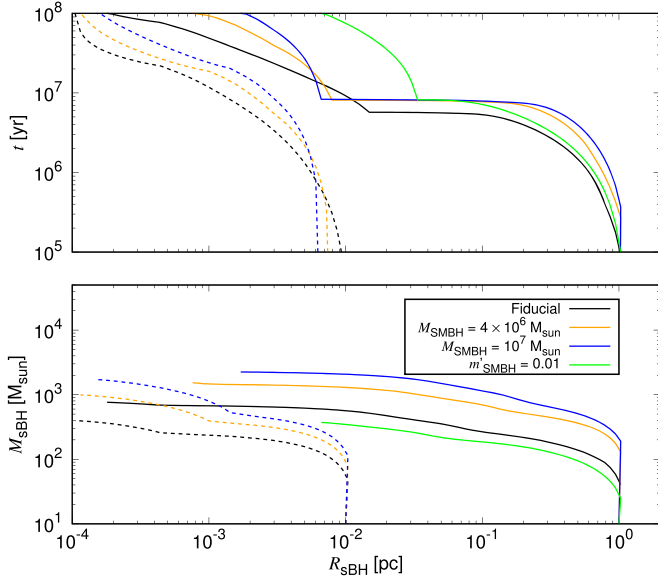
Figure 2. The time from the beginning of the AGN phase (top panel) for the sBH to grow to the mass M_{sBH} (bottom panel) for the fiducial model (black) as a function of the position R_{sBH}, assumed to be initially at $R_{ini} = 1$ pc (solid lines) and 0.01 pc (dotted lines), respectively. The results for an SMBH mass of $M_{SMBH} = 4 \times 10^6\, M_\odot$ (orange), for $10^7\, M_\odot$ (blue), and for the Eddington accretion rate of $\dot{m}_{SMBH} = 0.01$ (green) are also shown. The parameters of the fiducial model are given in Section 3.2 and Table 1.
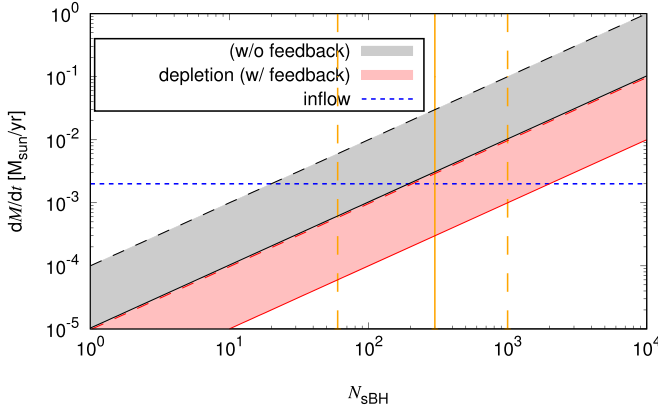

Figure 3. The depletion rate ($\dot{M}$) with (red) and without (black) the JFM for $t_{AGN} = 10$ Myr (dashed) to 100 Myr (solid), and the inflow rate from the outer boundary of the AGN disk (blue dashed) as a function of the number of sBHs (N_{sBH}) embedded in an AGN disk for $M_{SMBH} = 10^6\, M_\odot$ and $\dot{m}_{SMBH} = 0.1$. The y- and x-axes scale as $(M_{SMBH}/10^6\, M_\odot)(\dot{m}_{SMBH}/0.1)$ and $(\dot{m}_{SMBH}/0.1)^{1/2}$, respectively. The orange vertical lines show the fiducial value (solid) and rough upper and lower limits (dashed) for $N_{sBH}\dot{m}_{SMBH,-1}^{1/2}$. As the figure shows, the expected number, 60–1000, of sBHs embedded in the AGN disk can cumulatively accrete a comparable amount to, or even more than, the proposed SMBH accretion rate, thus starving the SMBH.

3. The inner CsBD accretes onto the sBH in a relatively short timescale ($t_{cons} \sim 300$ yr; Equation (11)), and accretion onto the sBH and jet production are quenched.
4. The AGN gas refills the hollow cavity in a longer timescale ($t_{re} \sim 5 \times 10^3$ yr; Equation (14)). A jet then turns on again, and the cycle restarts from step 1.

Due to the existence of the quenching phase and lower inflow rates onto the sBH in later episodes, the averaged accretion rate onto the sBH is reduced by ∼10–100 (Section 3.7, Appendix C).
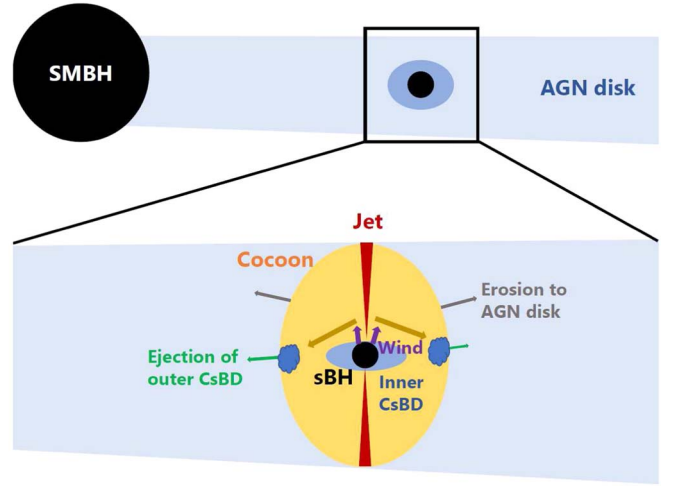

Figure 4. Schematic picture of the evolution of a cocoon produced around a jet.

Note that the relation $t_{break} \ll t_{cons} < t_{re}$ implies the presence of recurring intermittent accretion, rather than a steady state.

3.2. Numerical Choices

We set $M_{sBH,ini} = 10\, M_\odot$ since nuclear star clusters are rather metal-rich (e.g., Do et al. 2018; Schödel et al. 2020) and remnant masses are roughly predicted to come around this value owing to intense stellar mass loss (e.g., Belczynski et al. 2010). We assume that the initial radial position of the sBH is $R_{sBH,ini} = 1$ pc; the mass of the SMBH is $M_{SMBH} = 10^6\, M_\odot$; the gas inflow rate from the outer boundary ($R_{out} = 5$ pc) of the AGN disk in units of the Eddington rate is $\dot{m}_{SMBH} = 0.1$; the angular momentum transfer parameter of the AGN disk is $m_{AM} = 0.15$ (Thompson et al. 2005); the viscous parameter of the AGN disk is $\alpha_{AGN} = 0.1$ assuming partially ionized gas ($\gtrsim 10^3$ K) and that of the CsBD is $\alpha_{CsBD} = 0.3$ assuming fully ionized gas (King et al. 2007; Martin et al. 2019); the jet energy conversion efficiency is $\eta_j = 0.5$ (Appendix A.1); the opening angle of the injected jet is $\theta_0 = 0.2$, with the caveat that it is highly uncertain (e.g., Pushkarev et al. 2009; Hada et al. 2013, 2018; Berger 2014); and the reduction fraction of the accretion rate onto the sBH ($\dot{M}_{sBH}$) over the capture rate is $f_{acc} = \dot{M}_{sBH}/\dot{M}_{cap} = 0.1$, which is assumed to be due to mass loss by wind/outflows and episodic accretion as described in Section 3.6.

3.3. Jet and Cocoon

Here we briefly describe the properties of a jet and a surrounding cocoon. A relativistic jet is produced from a rotating sBH accreting at a super-Eddington rate (see Appendix A.1) owing to the BZ process with luminosity

$$L_j = \eta_j \dot{M}_{sBH} c^2$$
$$\simeq 10^{42} \text{ erg s}^{-1} \left(\frac{\dot{M}_{cap}}{3 \times 10^{-4}\, M_\odot \text{ yr}^{-1}}\right)\left(\frac{\eta_j}{0.5}\right)\left(\frac{f_{acc}}{0.1}\right), \quad (7)$$

where c is the speed of light.

Expressing L_j in terms of θ_0 and ρ_{AGN}, the properties of the cocoon, the head velocity (β_h), the cocoon velocity (β_c), the cocoon opening angle (θ_c), and pressure (P_c) are estimated as described in Appendix A.2.

3.4. Evaporation of the CsBD

To estimate the regulation of gas accretion as mediated by the evolution of the cocoon, it is crucial to understand how much gas in the AGN disk and the CsBD around the sBH is depleted after the cocoon propagation. Note that, in a constant density profile $\rho \propto z^0$, the cocoon also propagates laterally along the $z = 0$ plane (e.g., Wagner & Bicknell 2011; Bromberg et al. 2014), which likely results in an interaction with the CsBD. As the expanding cocoon hits the outer regions of the CsBD from above and below, the resulting shock heating can disrupt and unbind the outer regions of the disk. Due to the strong shocks, the pressure of the CsBD is roughly enhanced to the pressure of the cocoon (P_c). The approximation of the uniform pressure within the shock downstream works for the shock propagation in the case that the internal pressure of the shocked medium dominates over any external pressure (e.g., Kompaneets 1960). If the sound speed of the shocked CsBD ($\sim [P_c/\rho_{\rm CsBD}(r)]^{1/2}$) exceeds the escape velocity from the sBH at some distance R, the CsBD at distances $r > r_{\rm tru}$ is expected to be ejected (e.g., Perna et al. 2000), where $\rho_{\rm CsBD}(r)$ is the density of the CsBD at r before the shock heating and $r_{\rm tru}$ is the truncation radius. An estimate of $r_{\rm tru}$ can be made via the condition

$$\rho_{\rm CsBD}(r_{\rm tru})v_{\rm CsBD,Kep}(r_{\rm tru})^2 = P_c, \qquad (8)$$

where $v_{\rm CsBD,Kep}(r) = \sqrt{GM_{\rm sBH}/r}$ is the Keplerian velocity of the CsBD at a distance r from the sBH.

By solving Equation (8) with P_c (Equation (A4)), the truncation radius can be written as

$$r_{\rm tru} \sim 2 \times 10^{14}\ {\rm cm} \left(\frac{\rho_{\rm AGN}}{4 \times 10^{17}\ {\rm g\ cm^{-3}}}\right)^{-20/53}$$
$$\left(\frac{\beta_c}{0.03}\right)^{-40/53}\left(\frac{M_{\rm sBH}}{10\ M_\odot}\right)^{31/53}\left(\frac{\dot{M}_{\rm sBH}/\eta_{\rm rad}}{3 \times 10^{-4}\ M_\odot\ {\rm yr^{-1}}}\right)^{8/53}$$
$$\left(\frac{\alpha_{\rm CsBD}}{0.3}\right)^{-14/53}\left(\frac{\kappa_{\rm CsBD}}{2\ {\rm cm^2/g}}\right)^{-6/53} \qquad (9)$$

for gas pressure dominated regions of the CsBD (e.g., Haiman et al. 2009; black line of Figure 1(a)), where $\kappa_{\rm CsBD}$ is the opacity of the CsBD. The value of the opacity is consistently computed to satisfy the temperature and the density at $r_{\rm tru}$ for the standard disk model (Shakura & Sunyaev 1973), using the opacity functions given by Bell & Lin (1994). Within the photon trapping radius ($r_{\rm trap} \sim (3/2)r_g[\dot{M}_{\rm sBH}/\dot{M}_{\rm Edd}(M_{\rm sBH})\eta_{\rm rad}]$ for an accretion disk; e.g., Kato et al. 2008; brown line in Figure 1(a)), we instead adopt the slim-disk model, in which cooling is carried by advection (e.g., Kato et al. 2008), where r_g is the gravitational radius. When $r_{\rm trap} > r_{\rm tru}$, the cocoon truncates a slim disk, which is found to be the case when a gap is assumed not to form (dashed lines in Figure 1(a)). The CsBD's mass within $r_{\rm tru}$ is

$$M_{\rm CsBD,tru} \sim \pi r_{\rm tru}^2 \Sigma_{\rm CsBD}(r_{\rm tru})$$
$$\sim 0.01\ M_\odot \left(\frac{\rho_{\rm AGN}}{4 \times 10^{-17}\ {\rm g\ cm^{-3}}}\right)^{-28/53}\left(\frac{\beta_c}{0.03}\right)^{-56/53}$$
$$\left(\frac{M_{\rm sBH}}{10\ M_\odot}\right)^{54/53}\left(\frac{\dot{M}_{\rm sBH}/\eta_{\rm rad}}{3 \times 10^{-4}\ M_\odot\ {\rm yr^{-1}}}\right)^{43/53}$$
$$\left(\frac{\alpha_{\rm CsBD}}{0.3}\right)^{-62/53}\left(\frac{\kappa_{\rm CsBD}}{2\ {\rm cm^2/g}}\right)^{-19/53}, \qquad (10)$$

where $\Sigma_{\rm CsBD}(r)$ is the surface density of the CsBD at r.

We set the consumption timescale of $M_{\rm CsBD,tru}$ to

$$t_{\rm cons} = M_{\rm CsBD,tru}/\dot{M}_{\rm cap}$$
$$\sim 300\ {\rm yr} \left(\frac{M_{\rm CsBD,tru}}{0.01\ M_\odot}\right)\left(\frac{\dot{M}_{\rm cap}}{3 \times 10^{-4}\ M_\odot\ {\rm yr^{-1}}}\right)^{-1} \qquad (11)$$

(black line in Figure 1(b)), which is comparable to the viscous timescale at this radius. Here, for simplicity, we assume that the accretion rate onto the sBH is unchanged after the cocoon ejects the outer regions of the CsBD. This assumption ignores the outward diffusion of the CsBD and the possible enhancement of the accretion rate due to heating by the shock, while it does not affect the estimate of the averaged accretion rate, as long as the fraction $\sim f_{\rm acc}$ of the bounded CsBD ($M_{\rm CsBD,tru}$) is accreted onto the sBH within the resupply timescale ($t_{\rm re}$; Equation (14)). For simplicity, the change of $f_{\rm acc}$ after the truncation is ignored in our estimate.

3.5. Erosion of Cocoon

Next, we compute the radial extent from the sBH up to which the cocoon can propagate and eject gas in the AGN disk. This radial extent can be estimated by the Kompaneets method (Kompaneets 1960) for simple density profiles, by assuming a strong shock and uniform internal pressure within the shocked medium. Olano (2009) showed that shocks can laterally propagate to $r \lesssim \pi H_{\rm AGN}$ for spherical explosions produced at $z = Z = r = 0$ with a density profile of $\rho = \exp(-|Z|/H_{\rm AGN})$. Although the geometry of the cocoon and the density profiles in AGN disks may be different from those in Olano (2009), we approximately estimate the radial extent of the cocoon to be

$$r_{\rm dep} = f_{\rm ext}\,r_c$$
$$\sim 5 \times 10^{15}\ {\rm cm} \left(\frac{H_{\rm AGN}}{0.003\ {\rm pc}}\right)\left(\frac{\theta_c}{0.2}\right)\left(\frac{f_{\rm ext}}{3}\right) \qquad (12)$$

(orange line in Figure 1(a)), where $f_{\rm ext}$ accounts for the geometrical and ambient-profile effects and $r_c \sim H_{\rm AGN}\theta_c$ is the r-direction extent of the cocoon at the jet breakout, whose timescale is

$$t_{\rm break} \sim H_{\rm AGN}/(\beta_h c) \sim 0.05\ {\rm yr} \left(\frac{H_{\rm AGN}}{0.003\ {\rm pc}}\right)\left(\frac{\tilde{L}}{0.03}\right)^{-0.5} \qquad (13)$$

(blue line in Figure 1(b)). After the jet breakout, the cocoon also escapes in the vertical direction on a timescale that is of the same order as $t_{\rm break}$.

3.6. Resupply of Gas

After the cocoon escapes vertically from the AGN disk plane, gas outside $r_{\rm dep}$ is resupplied to the sBH. The resupply timescale of gas to the CsBD is roughly given by

$$t_{\rm re} \sim r_{\rm dep}/c_{s,\,{\rm AGN}}$$
$$\sim 5 \times 10^3\ {\rm yr} \left(\frac{r_{\rm dep}}{6 \times 10^{15}\ {\rm cm}}\right)\left(\frac{c_{s,{\rm AGN}}}{0.4\ {\rm km\ s^{-1}}}\right)^{-1} \qquad (14)$$

(orange line in Figure 1(b); e.g., Tanigawa et al. 2012). Gas inflow onto sBHs preferentially proceeds from the direction perpendicular to the AGN disk plane, as found in high-resolution three-dimensional hydrodynamical simulations (Ayliffe & Bate 2009; Tanigawa et al. 2012; Szulágyi et al. 2022). Such inflow structure

enables multiple episodes of cocoon evolution by ensuring interactions of the jets and inflowing gas.

In the following we make a rough estimate of the accretion rate onto the sBH after the resupply. According to the hydrodynamical simulation for gas flow onto a circumplanetary disk by Tanigawa et al. (2012), gas captured by the sBH vertically falls onto the CsBD with some angular momentum, and subsequently it quickly circularizes at the corresponding Keplerian radius. The total mass accretion rate onto the CsBD inside some distance r roughly follows:

$$\dot{M}_{\rm CsBD,Kep}(<r) \sim \begin{cases} \dot{M}_{\rm cap}(r/r_{\rm CsBD,out})^{0.5} \\ \qquad \text{for } r \lesssim r_{\rm CsBD,out}, \\ \dot{M}_{\rm cap} \quad \text{otherwise} \end{cases} \quad (15)$$

(Figure 14 of Tanigawa et al. 2012), where $r_{\rm CsBD,out}$ is the outer radius of the CsBD. We parameterize it as $r_{\rm CsBD,out} \sim f_{\rm circ} r_{\rm Hill}$, where $f_{\rm circ} = 0.1$–0.4 is inferred from simulations of circumplanetary disks (Ayliffe & Bate 2009; Martin & Lubow 2011; Tanigawa et al. 2012). The circularized gas inflows toward the sBH on the viscous timescale. Equating the viscous timescale to the resupply timescale, we can obtain the critical radius, $r_{\rm vis}$, beyond which the bulk of the gas cannot accrete within the resupply timescale. In the fiducial model, $r_{\rm vis} \sim 0.01\, r_{\rm Hill}$. Then, the gas inflow rate to the sBH within $r_{\rm vis}$ is reduced to

$$\dot{M}_{\rm in,vis} \sim \dot{M}_{\rm CsBD,Kep}(<r_{\rm vis}) \sim 0.3\, \dot{M}_{\rm cap}\left(\frac{f_{\rm circ}}{0.1}\right)^{-1/2}. \quad (16)$$

Note that the reconstituted CsBD can extend beyond $r_{\rm vis}$, but its outer regions, beyond this radius, will not have reached equilibrium during the disk accretion episodes. We assume that the reduction of the inflow rate of the CsBD in later episodes is effectively taken into account in $f_{\rm acc}$ (Section 3.2).

Once gas resupplies and accretion begins, we assume that jets are launched soon (on a timescale of $\lesssim 1$ s; e.g., Narayan et al. 2021; see also Appendix A.1).

3.7. Time-averaged Accretion Rate

The average accretion rate in units of the Eddington rate is estimated by multiplying the active fraction ($t_{\rm cons}/t_{\rm re}$; Figure 1(b)) as

$$\dot{m}_{\rm sBH,ave} = \min\left(1, \frac{t_{\rm cons}}{t_{\rm re}}\right)\frac{\dot{M}_{\rm sBH}}{\dot{M}_{\rm Edd}(M_{\rm sBH})}$$
$$\sim 10\left(\frac{\rho_{\rm AGN}}{4\times10^{-17}\,\rm g\,cm^{-3}}\right)^{-28/53}\left(\frac{\dot{M}_{\rm sBH}}{3\times10^{-5}\,M_\odot\,\rm yr^{-1}}\right)^{43/53}$$
$$\left(\frac{\beta_{\rm c}}{0.03}\right)^{-56/53}\left(\frac{M_{\rm sBH}}{10\,M_\odot}\right)^{1/53}\left(\frac{\eta_{\rm rad}}{0.1}\right)^{10/53}\left(\frac{f_{\rm acc}}{0.1}\right)$$
$$\left(\frac{\alpha_{\rm CsBD}}{0.3}\right)^{-62/53}\left(\frac{\kappa_{\rm CsBD}}{2\,\rm cm^2\,g^{-1}}\right)^{-19/53}\left(\frac{\theta_{\rm c}}{0.2}\right)^{-1}$$
$$\left(\frac{H_{\rm AGN}}{0.003\,\rm pc}\right)^{-1}\left(\frac{f_{\rm ext}}{3}\right)^{-1}\left(\frac{c_{\rm s,AGN}}{0.4\,\rm km\,s^{-1}}\right) \quad (17)$$

for $t_{\rm cons}/t_{\rm re} \leqslant 1$ on the right-hand side. In the fiducial setting, the accretion rate is reduced by a factor of ~ 60 ($t_{\rm re}/t_{\rm cons} \sim 20$ and a further reduction by ~ 3 due to the depletion of the inflow rate onto the sBH described in Section 3.6) compared to that without the JFM (another factor of ~ 3 is assumed to be reduced by wind/outflow feedback), and the accretion rate becomes
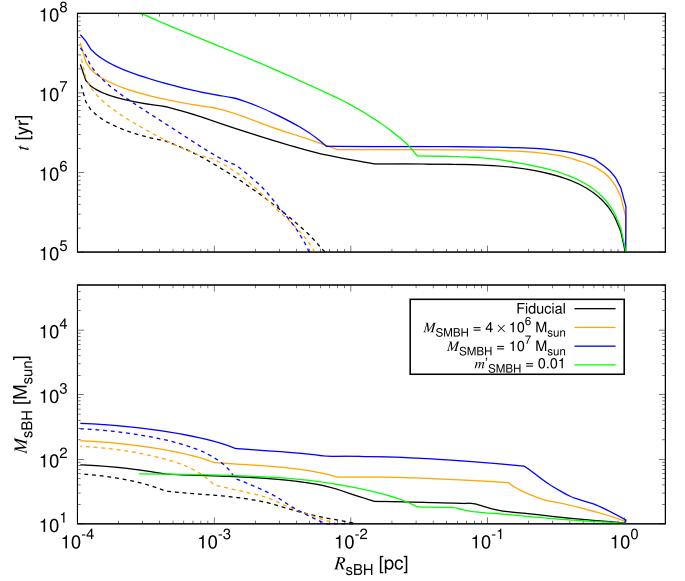

Figure 5. Same as Figure 2, but with the JFM. As the comparison of the two figures shows, the final sBH masses are reduced by approximately one order of magnitude.

moderately super-Eddington by a factor $\dot{M}_{\rm sBH}/\dot{M}_{\rm Edd}(M_{\rm sBH}) \sim 10$ (Equation (17), black line in Figure 1(c)).

4. Discussion

We now discuss the influence of the JFM on the overgrowth and depletion problems highlighted in Section 2. Figure 5 shows the evolution of the sBH in an AGN disk calculated in the same way as in Figure 2, but accounting for the JFM. With feedback, the growth of sBHs is suppressed compared to that without feedback (bottom panels of Figures 5 and 2). Although the average accretion rate shown in Figure 1(c) is still significant, especially in inner regions of $R_{\rm sBH} \lesssim 0.1$ pc, sBHs can open a gap at $R_{\rm sBH} \lesssim 0.01$ pc and the accretion rate is further reduced by a factor of $\sim 100(M_{\rm sBH}/100\,M_\odot)^2$ for massive sBHs (Figures 2, 5, and 8) compared to the black line of Figure 1(c). Here, in gap regions, the density of the AGN disk becomes lower, reducing the cocoon pressure and weakening the JFM. On the other hand, if a gap does not form as suggested by different disk models, the regulation by the cocoon is efficient in the inner regions of $R \lesssim 0.01$ pc, as a low-density inner slim CsBD is efficiently ejected (the dashed lines of Figure 1(c)) by the high-pressure cocoon in the high-density AGN disk. Due to the suppression of accretion, sBHs migrate to $R_{\rm sBH} \sim 10^{-4}$ pc almost without passing through the regions prohibited by the S2 orbits (Section 2; see also Gravity Collaboration et al. 2020). Hence, the overgrowth problem can be avoided.

Next, we consider the depletion problem. With

$$M_{\rm sBH,fin} \sim 100\,M_\odot\left(\frac{M_{\rm SMBH}}{10^6\,M_\odot}\right)\left(\frac{\dot{m}_{\rm SMBH}}{0.1}\right)^{1/2} \quad (18)$$

at $t_{\rm AGN} = 10$–100 Myr roughly derived from Figure 5 and Equation (3), the depletion rate is

$$\dot{M}_{\rm sBH,tot} \sim M_{\rm sBH,fin}N_{\rm sBH,AGN}/t_{\rm AGN}$$
$$\sim 3\times10^{-3} - 3\times10^{-4}\,M_\odot\,\rm yr^{-1}\left(\frac{M_{\rm SMBH}}{10^6\,M_\odot}\right)\left(\frac{\dot{m}_{\rm SMBH}}{0.1}\right),$$

which is smaller than the inflow rate of

$$\dot{M}_{\rm SMBH,in} \simeq 2 \times 10^{-3}\, M_\odot\, {\rm yr}^{-1} \left(\frac{M_{\rm SMBH}}{10^6\, M_\odot}\right)\left(\frac{\dot{m}_{\rm SMBH}}{0.1}\right) \quad (19)$$

in later phases of $t_{\rm AGN} \gtrsim$ a few $\times$ 10 Myr with the same dependence (Figure 3). Note that the ejection mass of gas orbiting above the sBH (with the density $\rho_{\rm AGN}$) is calculated to be smaller in most cases than the mass accreted by the sBH (see Appendix C), so that this ejected gas does not exacerbate the depletion problem. Also, the ejected CsBDs can be recaptured by the AGN disk. The radius within which the sonic velocity after shock heating by the cocoon is lower than the escape velocity from the SMBH ($r_{\rm esc}$) exceeds the CsBD size ($r_{\rm CsBD,out}$) for

$$R_{\rm sBH} \gtrsim 0.1\, {\rm pc} \left(\frac{f_{\rm circ}}{0.1}\right)\left(\frac{M_{\rm SMBH}}{10^6\, M_\odot}\right)\left(\frac{\dot{m}_{\rm SMBH}}{0.1}\right) \quad (20)$$

in the fiducial settings. For $M_{\rm SMBH} \sim 10^6\, M_\odot$, the condition $\dot{M}_{\rm sBH,tot} < \dot{M}_{\rm inflow}$ is marginally satisfied, while for $M_{\rm SMBH} \lesssim 10^5\, M_\odot$ inflowing gas may be depleted by the JFM, as the ejected CsBDs often escape. Interestingly, the regulation by the JFM may be consistent with observations indicating that high-Eddington-ratio AGNs are rare for $M_{\rm SMBH} \lesssim 10^5\, M_\odot$ (Greene & Ho 2007). In either case, the depletion problem can be alleviated by the JFM.

Our results depend on several assumptions. First, we assumed the fraction of the outer radius of the CsBD over the Hill radius ($f_{\rm circ} = r_{\rm CsBD,out}/r_{\rm Hill}$), $\dot{M}_{\rm CsBD,Kep}(<r)$, and we relied on a gas inflow geometry derived in studies of protoplanetary systems. Second, $f_{\rm ext}$ and $r_{\rm tru}$ are roughly determined by assuming uniform pressure inside the shocked medium. Third, hydrodynamical jets are assumed to be produced once super-Eddington accretion onto a spinning sBH is realized. The regulation of accretion by the cocoon can be drastically influenced by the failure of these assumptions. If it fails, a possible alternative process for regulation would be that of a significant outflow compared to inflow on the sBHs—i.e., suggesting that highly super-Eddington accretion is self-regulated. Thus, AGN disks can be good experimental environments to understand the processes regulating highly super-Eddington accretion flows.

5. Conclusions

In this paper, for the first time, we considered the jet feedback mechanism for regulating gas accretion onto sBHs in AGN disks, in which a cocoon generated around a jet launched by an accreting sBH due to the BZ effect can regulate the average accretion onto the sBH over the AGN lifetime. Additionally, we find that a similar regulation can occur in the outer regions of the AGN disk owing to winds from the embedded sBHs (Appendix B.3). Our main results are summarized as follows:

1. We highlight two problems for gas accretion onto sBHs in AGN disks. One is the overgrowth of sBHs, and the other is the depletion of gas inflow in AGN disks by the population of sBHs in the disk, starving the central SMBH.
2. Due to the cocoon evolution, the accretion rate onto sBHs embedded in AGN disks is reduced by a factor of ~10–100, depending on parameters.

3. The problems of the depletion of gas inflow and overgrowth of massive sBHs can be avoided by considering the jet feedback mechanism.
4. Efficient gas ejection and depletion of gas inflow in AGN disks around less massive SMBHs of $\lesssim 10^5\, M_\odot$ expected by the jet feedback mechanism may explain the dearth of quasars with high accretion rates for such SMBHs.

These findings suggest that cocoons play a significant role in regulating accretion in AGN disks and the evolution of embedded compact objects. Finally, we note that shocks produced by winds from CsBDs also play a role in regulating accretion in the outer regions $R \gtrsim 10^{-1}$ pc of the AGN disk.

Appendix A
Mechanisms

Here we provide further details on the mechanisms related to the regulation of gas accretion by the cocoon.

A.1. Jet Production

We outline how a jet is launched from an accreting sBH embedded in an AGN disk. In the AGN disk, an sBH is surrounded by a CsBD (Figure 4). When the CsBD is advection dominated, as expected here, a magnetically dominated state can be realized (e.g., Meier 2001; Kimura et al. 2021b) owing to the accumulation of the magnetic flux in the vicinity of the sBH (Cao 2011). Even if the magnetic flux is initially weak, the outflow from the disk converts the toroidal magnetic field generated by the shear motion into a poloidal field (Liska et al. 2020). Such advection-dominated flows are expected for super-Eddington accretion rates (Abramowicz et al. 1988) or low accretion rates of $\dot{M}_{\rm sBH} \lesssim 0.01\, \dot{M}_{\rm Edd}(M_{\rm sBH})$ (e.g., Narayan & Yi 1994; Blandford & Begelman 1999). In these cases, the jets from spinning BHs can be launched through the BZ process (Blandford & Znajek 1977). We assume that the luminosity of the relativistic jet is proportional to the mass accretion rate onto the sBH as

$$L_j = \eta_j \dot{M}_{\rm sBH} c^2 \quad (A1)$$

(Blandford & Znajek 1977). Note that the jet is assumed to be launched once accretion begins owing to efficient magnification of the magnetic field during gas inflow (Cao 2011). On the other hand, if the launch of the jet is delayed by a timescale longer than the consumption timescale $t_{\rm cons}$, then the average accretion rate onto the sBH is enhanced by the ratio of those timescales compared to Equation (17). Here η_j is approximated as $\eta_j \sim a_{\rm sBH}^2$ for a magnetically dominated state (e.g., Tchekhovskoy et al. 2010, 2011; Narayan et al. 2021). In the fiducial model, we adopt the conversion efficiency to the jet to be $\eta_j = 0.5$, assuming a merger remnant with a dimensionless

spin of $a_{\rm sBH} \sim 0.7$ (e.g., Buonanno et al. 2008; a different value for η_j is investigated in Appendix C.1). We ignore the spin evolution of sBHs by gas accretion and production of the BZ jet (Narayan et al. 2021), which affects η_j and accordingly the regulation rate of accretion by the cocoon. In our model, a jet is assumed to be launched whenever $\dot{M}_{\rm sBH} > \dot{M}_{\rm Edd}$.

A.2. Cocoon Propagation

We describe the properties of the cocoon evolving in the AGN disk following the formalism of Bromberg et al. (2011), who investigate hydrodynamic jets. Although a BZ jet is considered to be an initially magnetized jet, we adopt the formulae for hydrodynamic jets for simplicity.

When the jet collides with the AGN disk orbiting above an sBH, two shocks form: a forward shock propagating in the AGN disk and a reverse shock in the jet. The region sandwiched by the two shocks is called the jet head. The head velocity is estimated as

$$\beta_h \sim \begin{cases} \widetilde{L}^{1/2} & \text{for } \widetilde{L} < 1, \\ 1 & \text{otherwise,} \end{cases} \quad (A2)$$

where

$$\widetilde{L} \sim \begin{cases} \left(\dfrac{L_j}{\rho_{\rm AGN} t_j^2 \theta_0^4 c^5}\right)^{2/5} & \text{for } \widetilde{L} < \theta_0^{-4/3}, \\ \dfrac{L_j}{\rho_{\rm AGN} t_j^2 \theta_0^2 c^5} & \text{otherwise} \end{cases} \quad (A3)$$

is the ratio between the energy density of the jet and the rest-mass energy density of the surrounding medium at the location of the head, where t_j is the time since the jet is launched.

If the energy stored in the cocoon (E_c) is uniformly distributed within the cocoon's volume (V_c), the pressure of the cocoon is

$$P_c = E_c/3V_c \sim \begin{cases} \widetilde{L}\theta_0^2 \rho_{\rm AGN} c^2 & \text{for } \widetilde{L} < \theta_0^{-4/3}, \\ \widetilde{L}^{1/4}\theta_0 \rho_{\rm AGN} c^2 & \text{for } \theta_0^{-4/3} < \widetilde{L} < 4\Gamma_j^4, \\ \Gamma_j \theta_0 \rho_{\rm AGN} c^2 & \text{otherwise.} \end{cases} \quad (A4)$$

where Γ_j is the Lorentz factor just below the head. In Equation (A4), it is assumed that the radiation pressure dominates the gas pressure, which is valid as long as the cocoon is optically thick, since the cocoon has a high temperature, and the radiation and gas pressures evolve following a similar scaling in the adiabatic phase (e.g., Kashiyama et al. 2013). Note that in the optically thin regimes (dashed orange line in Figure 7(b)) the Coulomb timescale (dashed black line in Figure 7(c)) is longer than the breakout timescale (blue line in Figure 1(b)), implying that cooling is negligible for the cocoon evolution. In such regions, the gas pressure likely dominates the radiation pressure, and the cocoon pressure is given by $P_c = 2E_c/3V_c$. For instance, we calculated that the enhancement of the cocoon pressure by a factor of 2 reduces the final sBH mass (e.g., Figure 5) by a factor of ~ 1.3 in the fiducial model.

The lateral expansion velocity of the cocoon is

$$\beta_c = \sqrt{P_c/\rho_{\rm AGN}c^2} \sim \begin{cases} \widetilde{L}^{1/2}\theta_0 & \text{for } \widetilde{L} < \theta_0^{-4/3}, \\ \widetilde{L}^{1/8}\theta_0^{1/2} & \text{for } \theta_0^{-4/3} < \widetilde{L} < 4\theta_0^{-4}, \\ 1 & \text{otherwise,} \end{cases} \quad (A5)$$

and the opening angle of the cocoon is

$$\theta_c \sim \beta_c/\beta_h \sim \begin{cases} \theta_0 & \text{for } \widetilde{L} < 1, \\ \widetilde{L}^{1/2}\theta_0 & \text{for } 1 < \widetilde{L} < \theta_0^{-4/3}, \\ \widetilde{L}^{1/8}\theta_0^{1/2} & \text{for } \theta_0^{-4/3} < \widetilde{L} < 4\theta_0^{-4}, \\ 1 & \text{otherwise.} \end{cases} \quad (A6)$$

At breakout of the cocoon from the AGN disk ($t_j = \frac{H_{\rm AGN}}{\beta_h c}$), from Equations (A2) and (A3) we obtain

$$\widetilde{L} \sim \begin{cases} \left(\dfrac{L_j^2}{\rho_{\rm AGN}^2 \theta_0^8 c^6 H_{\rm AGN}^4}\right)^{1/3} & \text{for } \widetilde{L} < 1, \\ \left(\dfrac{L_j}{\rho_{\rm AGN} \theta_0^4 c^3 H_{\rm AGN}^2}\right)^{2/5} & \text{for } 1 < \widetilde{L} < \theta_0^{-4/3}, \\ \dfrac{L_j}{\rho_{\rm AGN} \theta_0^2 c^3 H_{\rm AGN}^2} & \text{otherwise.} \end{cases} \quad (A7)$$

With the fiducial values at $R = 1$ pc (Table 1), this becomes

$$\widetilde{L} \simeq 0.03 \left(\dfrac{L_j}{10^{42} \text{ erg s}^{-1}}\right)^{2/3} \left(\dfrac{\rho_{\rm AGN}}{4 \times 10^{-17} \text{ g cm}^{-3}}\right)^{-2/3}$$
$$\times \left(\dfrac{H_{\rm AGN}}{0.003 \text{ pc}}\right)^{-4/3} \left(\dfrac{\theta_0}{0.2}\right)^{-8/3}, \quad (A8)$$

and accordingly, $\beta_h \simeq 0.2(\widetilde{L}/0.03)^{1/2}$, $\beta_c \simeq 0.04(\widetilde{L}/0.03)^{1/2}$ $(\theta_0/0.2)$, and $\theta_c \sim 0.2(\theta_0/0.2)$. Thus, the properties of the cocoon are estimated by L_j, $\rho_{\rm AGN}$, $H_{\rm AGN}$, and θ_0.

A.3. Evolution of Black Hole Mass and Location

The time evolution of the mass for an sBH initially at the position $R_{\rm sBH}(t=0) = R_{\rm ini}$ and mass $M_{\rm sBH}(t=0) = M_{\rm sBH,ini}$ without feedback is calculated as

$$M_{\rm sBH}(t) = M_{\rm sBH,ini} + \int_0^t \dot{M}_{\rm cap}(R_{\rm sBH}(t'), M_{\rm sBH}(t'))dt', \quad (A9)$$

while the sBH time-dependent position within the AGN disk is calculated as

$$R_{\rm sBH}(t) = R_{\rm ini} - \int_0^t dt' R_{\rm sBH}(t')/t_{\rm mig}(R(t'), M_{\rm sBH}(t')), \quad (A10)$$

where $t_{\rm mig}$ is the migration timescale, for which we adopt Equation (A11) in the next section. Figures 2, 5, 8, and 9 are calculated using Equations (A9) and A10.

A.4. Migration

To calculate how sBHs migrate radially toward the central SMBH (Equation (A10), Figures 2 and 5(a)), we adopt the formulae for the timescale of migration of sBHs as

$$t_{\rm I,II} = \dfrac{\Sigma_{\rm disk}}{\Sigma_{\rm disk,min}} t_{\rm I} \quad (A11)$$

(Duffell et al. 2014; Kanagawa et al. 2018), where t_I is the type I migration timescale, given by

$$t_I \simeq \frac{1}{2f_{mig}}\left(\frac{M_{SMBH}}{M_{sBH}}\right)\left(\frac{M_{SMBH}}{\Sigma_{disk}R_{sBH}^2}\right)\left(\frac{H_{AGN}}{R_{sBH}}\right)^2\Omega_{Kep}^{-1} \quad (A12)$$

(e.g., Ward 1997; Tanaka et al. 2002; Paardekooper et al. 2010; Baruteau et al. 2011), where Σ_{disk} is the surface density of the AGN disk, Ω_{Kep} is the Keplerian angular velocity around the SMBH, and f_{mig} is a dimensionless factor depending on the local temperature and density profiles (see Paardekooper et al. 2010; Baruteau et al. 2011). We set $f_{mig} = 2$ in the fiducial model, which is the typical value numerically found by Kanagawa et al. (2018). Fung et al. (2014) and Kanagawa et al. (2015) estimated that, due to the gravitational torque from a migrator, the surface density in the disk annulus at the migrator's orbit is reduced to

$$\Sigma_{disk,min} = \frac{\Sigma_{disk}}{1 + 0.04K}, \quad (A13)$$

where

$$K = (M_{sBH}/M_{SMBH})^2(H_{AGN}/R_{sBH})^{-5}\alpha_{eff}^{-1}, \quad (A14)$$

and $\alpha_{eff} = \nu/(c_{s,AGN}H_{AGN})$ is the effective α viscosity parameter. In the outer regions of AGN disks where angular momentum transfer is presumed to be driven by torques from stellar bars, spiral waves, or large-scale magnetic stresses, this parameter is given by $\alpha_{eff} = m_{AM}R/H_{AGN}$.

For reference, it would be useful to present the typical sBH mass above which migration becomes efficient. If we assume $\dot{M}_{sBH,ave} = \dot{M}_{cap}f_{acc,eff}$ with a constant $f_{acc,eff}$, since the capture timescale ($t_{acc} = M_{sBH}/\dot{M}_{sBH,ave} \propto M_{sBH}^{1/3}$) weakly depends on M_{sBH} compared to the migration timescale ($t_I \propto M_{sBH}$) in the fiducial model, there is a critical mass above which the sBH efficiently migrates in cases without gaps (Tanaka et al. 2020). By equating Equations (1) and (A12), the critical mass at which $t_{acc} = t_I$ is

$$M_{crit} = M_{SMBH}[f_{acc,eff}(1/3)^{2/3}$$
$$\times (f_c/4f_{mig})(H_{AGN}/R_{sBH})^2]^{3/4}$$
$$\sim 1.1 \times 10^{-4} M_{SMBH}\left(\frac{f_{acc,eff}}{1}\right)^{3/4}\left(\frac{f_c}{10}\right)^{3/4}$$
$$\times \left(\frac{f_{mig}}{2}\right)^{-3/4}\left(\frac{H_{AGN}/R_{sBH}}{0.003}\right)^{3/2}. \quad (A15)$$

Since $f_{acc,eff}$ is 1 and $\sim 1/60$ without and with the JFM at $R_{sBH} = 1$ pc, respectively, the critical mass is $\sim 100\,M_\odot\,(M_{SMBH}/10^6\,M_\odot)$ and $\sim 5\,M_\odot\,(M_{SMBH}/10^6\,M_\odot)$, which are roughly consistent with the turning points of the lines in the bottom panels of Figures 2 and 5. It is found from Equation (A15) that as H_{AGN}/R_{sBH} increases, the growth of the sBH becomes efficient compared to the migration. Then, stronger feedback (lower $f_{acc,eff}$) presumably becomes required to resolve the overgrowth problem.

Appendix B
Feedback

B.1. Influence on Gas Inflow

While sBHs are accreting, several kinds of feedback possibly affect the gasdynamics: (i) radiation pressure inside the CsBD and wind/outflow from a thick disk or line-driven wind, (ii) thermal pressure of ionized gas, (iii) radiation pressure on dust by infrared photons, (iv) dynamical instabilities, and (v) gap formation. We evaluate whether these processes can regulate gas accretion onto sBHs in AGN disks.

(i) When the accretion rate exceeds the Eddington rate, the radiation pressure on ionized gas exceeds the gravity from the sBH, which can regulate gas accretion (while accretion might be promoted by the positive JFM for nearly spherical flows; Chamandy et al. 2018). However, in such highly accreting cases, cooling of the CsBD in the vicinity of the sBH is dominated by advection (neglecting neutrino cooling, which is efficient only for extremely rapid accretion with rates of $\gtrsim 10^4\,M_\odot\,yr^{-1}$; e.g., Di Matteo et al. 2002; Janiuk et al. 2004; Kohri et al. 2005; Chen & Beloborodov 2007). Then, photons can be trapped into the accretion flow and be accreted onto the sBH or escape in the vertical direction with respect to the CsBD (e.g., Jiang et al. 2014; Sadowski et al. 2015). In such highly accreting flows, wind/outflow feedback also pushes back the accreting gas. If the wind is isotropically emitted, it significantly regulates accretion (Wang et al. 2021a) and gasdynamical friction (Gruzinov et al. 2020). On the other hand, if it is anisotropic, as predicted by numerical simulations (Jiao et al. 2015; Kitaki et al. 2021), the feedback does not efficiently regulate either accretion (Takeo et al. 2020) or dynamical friction (Li et al. 2020). Also, when the trapping radius is smaller than the circularization radius, the mass ratio of outflows to inflows is modest (Kitaki et al. 2021).

If the outflow rate is much higher than the accretion rate onto the sBH due to wind (e.g., $f_{acc} \lesssim 0.01$; Blandford & Begelman 1999; Pan & Yang 2021), the overgrowth problem can be avoided, while the depletion problem is not resolved unless the wind is decelerated. This is because the wind velocity at launch (Section B.2) exceeds the escape velocity from the SMBH ($v_{esc} = (2GM_{SMBH}/R_{sBH})^{1/2}$) for

$$R_{sBH} \gtrsim 3 \times 10^{-4}\,pc\left(\frac{M_{SMBH}}{10^6\,M_\odot}\right)\left(\frac{\dot{m}_{sBH}}{10^5}\right). \quad (B1)$$

This condition is satisfied most of the time during the evolution of sBHs in AGN disks, and the wind does not decelerate when it is driven continuously and gas above the sBH is ejected. As a result, even though the significant outflows in CsBDs can prevent the sBHs from growing overly massive, the AGN disk is still depleted, because the outflowing material is unbound and ejected, rather than retained in the AGN disk. On the other hand, the feedback by thermalized winds remains to be investigated in detail. In Appendix B.3, we estimate regulation of accretion onto the sBH by these thermal winds.

(ii) The thermal pressure of H II regions formed by radiation from the accreting sBHs can push back the gas accreting onto the sBHs themselves and thus reduce the accretion rate (Milosavljević et al. 2009; Park & Ricotti 2011, 2012). On the other hand, when the size of H II regions around the sBHs (Strömgren radius, r_{HII}) is less than r_{BHL}, the dynamics of accreting gas is less influenced by the pressure (Inayoshi et al. 2016;

Toyouchi et al. 2020). The condition $r_{\rm HII} < r_{\rm BHL}$ is satisfied for sBHs corotating with the AGN disk at $r \lesssim$ a few parsecs, by considering the effect of dust opacity on absorption (e.g., Toyouchi et al. 2019) in solar or supersolar metallicity in AGN disks (e.g., Xu et al. 2018). Also, due to the shadow by the thick accretion disk, photons escape in the vertical direction (Sugimura et al. 2017), and then the H II regions are confined within $r \sim z \lesssim H_{\rm AGN}$. Under these conditions, the gasdynamics during capture by the sBH at $r \sim r_{\rm Hill}$ is less affected by the pressure of H II regions. However, since the geometry of the system is complex for gas inflow onto sBHs in AGN disks, the effect of radiation may be significantly different. We investigate the influence of the possible reduction of the gas density above the sBH by radiation or wind on the regulation of gas accretion in Appendix C. Also, in later episodes, gas inflows during quiescent phases. Due to the quick recombination in the dense AGN disks, we simply assume that gas quickly returns to the neutral state, justifying the resupply timescale (Equation (14)) assuming that gas moves to fill the cavity at the local sound speed of the AGN disk $c_{s,\rm AGN}$.

(iii) In AGN disks outside the dust sublimation radius,

$$R_{\rm sub} \sim 0.04 \; {\rm pc} \left(\frac{L_{\rm UV}}{10^{43} \; {\rm erg \; s}^{-1}} \right)^{1/2} \left(\frac{T_{\rm dust}}{1500 \; {\rm K}} \right)^{-2.8} \quad (B2)$$

(Barvainis 1987), where $L_{\rm UV}$ is the ultraviolet luminosity of the AGN and $T_{\rm dust}$ is the temperature at which grains are destroyed, the radiation pressure on dust by infrared photons may regulate accretion for high-metallicity environments (Toyouchi et al. 2019) without preventing gasdynamical friction (Toyouchi et al. 2020). On the other hand, when the ultraviolet radiation from the sBH is anisotropic owing to the shadow by the thick CsBD, this process does not regulate gas accretion (Toyouchi et al. 2021). Additionally, while being captured by the sBH, the gas experiences shocks (Lubow et al. 1999; Tanigawa et al. 2012), and dust in the CsBD is likely sublimated.

(iv) The captured gas can fragment if the CsBD becomes gravitationally unstable. Figure 6 shows the critical accretion rate above which the CsBD becomes Toomre unstable (the Toomre parameter becomes $Q < 1$) as a function of R. Hydrodynamical simulations for protoplanetary disks (Ayliffe & Bate 2009; Tanigawa et al. 2012) suggest $r_{\rm CsBD,out} \sim f_{\rm circ} r_{\rm Hill}$ with $f_{\rm circ} \sim 0.1$–0.4, corresponding to

$$r_{\rm CsBD,out} \sim 4 \times 10^{15} \; {\rm cm} \left(\frac{f_{\rm circ}}{0.1} \right) \left(\frac{R_{\rm sBH}}{\rm pc} \right)$$
$$\times \left(\frac{M_{\rm sBH}}{10 \; M_\odot} \right)^{1/3} \left(\frac{M_{\rm SMBH}}{10^6 \; M_\odot} \right)^{-1/3}. \quad (B3)$$

From Figure 6, the CsBD at $r_{\rm CsBD,out}$ becomes unstable roughly at

$$R_{\rm sBH} \gtrsim {\rm pc} \left(\frac{\alpha_{\rm CsBD}}{0.1} \right)^{c_0} \left(\frac{f_{\rm circ}}{0.1} \right)^{-1}$$
$$\times \left(\frac{M_{\rm sBH}}{10 \; M_\odot} \right)^{-1/3} \left(\frac{M_{\rm SMBH}}{10^6 \; M_\odot} \right)^{1/3} \quad (B4)$$

with $c_0 \sim 1/2$. When the CsBD becomes unstable, $\alpha_{\rm CsBD}$ is expected to be enhanced to $\sim O(1)$ owing to gravitational instability, and fragmentation may also occur (e.g., Kratter & Lodato 2016).
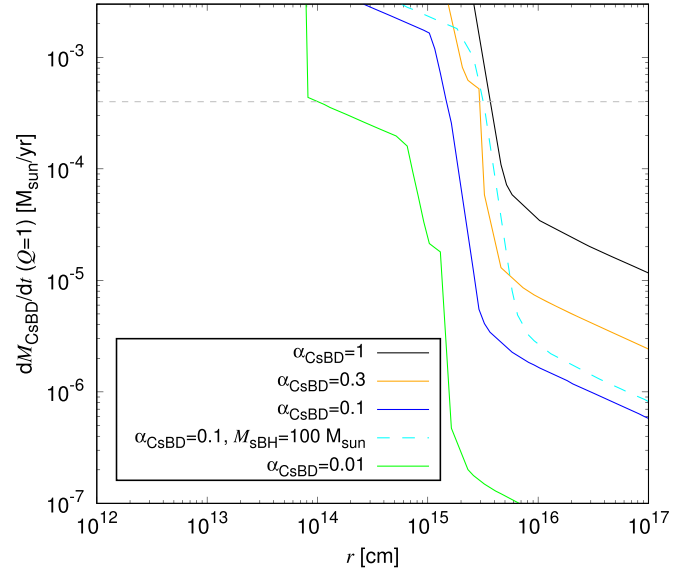

Figure 6. The accretion rate at which the Toomre parameter becomes 1 for several $\alpha_{\rm CsBD}$ and $M_{\rm sBH}$. The dashed gray line shows the gas capture rate by an sBH in the fiducial model.

If $r_{\rm CsBD,out} \gtrsim 10^{16}$ cm, the CsBD is unstable even if $\alpha_{\rm CsBD} \sim 1$, and the inflow rate may be reduced to several $\times 10^{-5} \; M_\odot \; {\rm yr}^{-1}$ (black line), although the degree of fragmentation and migration of fragments is not obvious. Thus, dynamical instability is expected and may reduce the gas accretion rate only in the outer regions at $R_{\rm sBH} \gtrsim$ pc.

(v) As described in Section A.4, a gap is predicted to form around the sBH in an AGN disk when K (Equation (A14)) becomes larger than ~ 20. This condition is satisfied for $R_{\rm sBH} \lesssim 0.01$ pc in the fiducial model. After the formation of the gap, the growth rate of the sBH is significantly reduced (Figures 2 and 5). Note that, by considering the evolution of many sBHs, deeper gaps are presumed to form owing to the sum of their torques at the same radial position, and then the growth of sBHs may be further suppressed especially in $R_{\rm sBH} \lesssim 0.01$ pc. Such N-body effects on the gap formation will be worth investigating in a future study.

Overall, the significant fraction of mass loss via winds (e.g., Jiang et al. 2014; Sadowski et al. 2015) might reduce the accretion rate onto an sBH, although it is suggested to be modest (Kitaki et al. 2021). Also, the inflow rate of the CsBD may be reduced by Toomre instability in outer regions of $R_{\rm sBH} \gtrsim$ pc and by gap formation in the inner regions with $R_{\rm sBH} \lesssim 0.01$ pc. Hence, without additional regulation processes, sBHs embedded in AGN disks presumably evolve to IMBHs especially for $R_{\rm sBH} \sim 0.01$–1 pc (Section 2).

B.2. Influence of Winds on Cocoon Evolution

The cocoon dynamics may be also influenced by the winds launched in super-Eddington regimes (e.g., Jiao et al. 2015; Kitaki et al. 2021). To evaluate this influence, we compare the pressure of the wind to that of the cocoon. The ram pressure of the wind at elevation z is

$$\rho_w v_w^2 = \frac{\dot{M}_w v_w}{\Omega_w z^2} \sim 20 \; {\rm erg \; cm}^{-3} \left(\frac{\dot{M}_w}{3 \times 10^{-5} \; M_\odot \; {\rm yr}^{-1}} \right)$$
$$\times \left(\frac{\beta_w}{0.03} \right) \left(\frac{z}{10^{14} \; {\rm cm}} \right)^{-2} \left(\frac{\Omega_w}{2\pi} \right)^{-1}, \quad (B5)$$
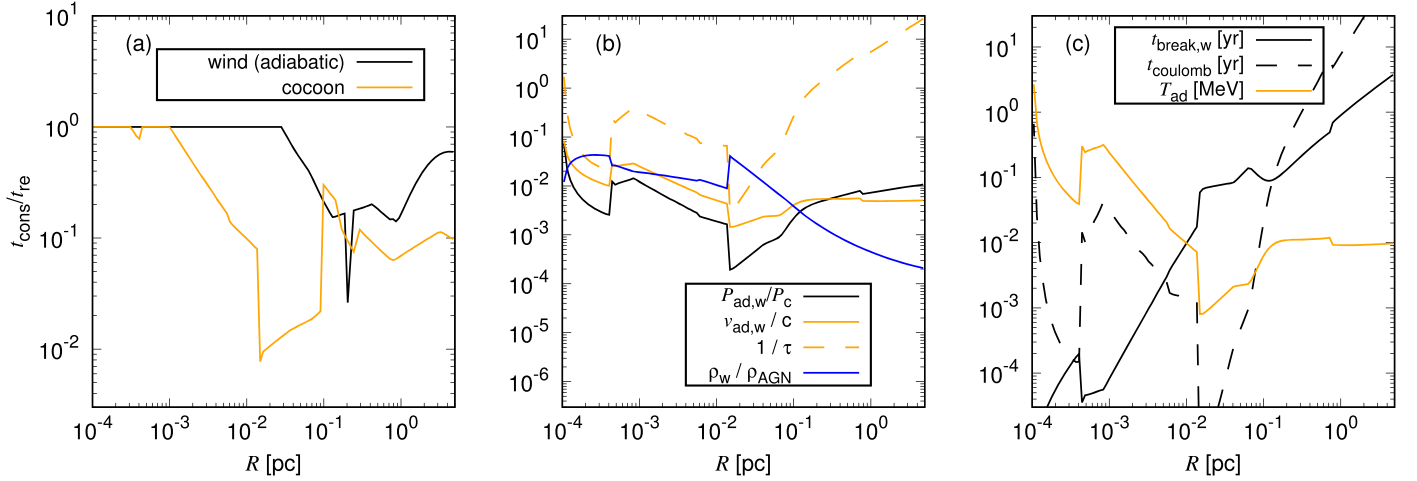
Figure 7. Various properties related to the shock produced by the wind as a function of R. (a) The reduction rate of accretion onto the sBH by the cocoon (orange) and by the wind shock without cooling (black). (b) The ratio of the thermal pressure with the temperature T_{ad} of the wind shock over the internal pressure of the cocoon (black), the dimensionless shock velocity at breakout assuming adiabatic evolution (solid orange; $v_{ad,w}/c$), the dimensionless photon diffusion velocity from the AGN disk (dashed orange; $1/\tau = 1/2\rho_{AGN}H_{AGN}\kappa_{AGN}$), and the ratio of the wind density at $z = H_{AGN}$ to the AGN density (blue). (c) The breakout timescale of the wind assuming adiabatic evolution (solid black), the Coulomb loss timescale for protons by collisions with electrons in the shock (dashed black), and the proton temperature of the shocked fluid assuming inefficient cooling (orange). In the case of the wind shock, accretion is regulated at $R \gtrsim 0.1$ pc, where cooling is inefficient.

where ρ_w is the wind density, $v_w = \beta_w c$ is the wind velocity, and Ω_w is the solid angle within which the wind is emitted at the inner region of the accretion disk. We assume that $\dot{M}_w \sim \dot{M}_{in,vis} - \dot{M}_{sBH}$. We approximate the wind velocity to be $\sim (m_{sBH}G/r_{trap})^{1/2} \sim [\dot{M}_{sBH}\eta_{rad}/\dot{M}_{Edd}(M_{sBH})]^{-1/2}c$ (e.g., Kitaki et al. 2021).

On the other hand, the cocoon pressure for $\tilde{L} < 1$ is

$$P_c = \tilde{L}\theta_0^2 \rho_{AGN}c^2 \sim 40 \text{ erg cm}^{-3} \left(\frac{\tilde{L}}{0.03}\right)$$
$$\times \left(\frac{\theta_0}{0.2}\right)^2 \left(\frac{\rho_{AGN}}{4 \times 10^{-17} \text{ g cm}^{-3}}\right). \quad (B6)$$

By equating Equations (B5) and (B6), the pressures become comparable at the equilibrium height of

$$z_{eq} \sim 8 \times 10^{13} \text{ cm} \left(\frac{\dot{M}_w}{3 \times 10^{-5} M_\odot \text{ yr}^{-1}}\right)^{1/2} \left(\frac{\beta_w}{0.03}\right)^{1/2}$$
$$\times \left(\frac{\Omega_w}{2\pi}\right)^{-1/2} \left(\frac{\tilde{L}}{0.03}\right)^{-1/2}$$
$$\times \left(\frac{\theta_0}{0.2}\right)^{-1} \left(\frac{\rho_{AGN}}{4 \times 10^{-17} \text{ g cm}^{-3}}\right)^{-1/2}. \quad (B7)$$

In the fiducial setting, z_{eq} is somewhat smaller than the truncation radius (Equation (9)), i.e., by a factor of several in no gap-forming regions (cyan line in Figure 1(a)). In this case ($z_{eq} < r_{tru}$), the cocoon can interact with and heat the CsBD at $r = r_{tru}$ without being inhibited by the wind pressure.

Even when $z_{eq} > r_{tru}$, the truncation radius is presumably unaffected by the wind. The wind pressure decreases with r, and the cocoon may be able to reach the disk midplane at $r \gtrsim z_{eq} > r_{tru}$. Then, the shock propagates to the inner part ($r_{tru} < r < z_{eq}$) of the CsBD and eventually arrives at $r = r_{tru}$. Also, a large fraction of the momentum by the wind is presumably confined within some solid angle from a polar axis (Jiao et al. 2015; Kitaki et al. 2021), and then winds do not affect cocoon dynamics around the midplane.

When the sBH is slowly spinning, the jet efficiency (η_j) becomes low and feedback is presumed to be dominated by the wind at some point. If $\eta_j \sim a_{sBH}^2$ is lower than $\sim f_w(v_w/c)^2 \sim f_w(\dot{m}_{sBH}\eta_{rad})^{-1}$, where $f_w = \dot{M}_w/\dot{M}_{cap}$ is the fraction of the wind-loss rate over the capture rate, the luminosity of the jet roughly becomes lower than that of the wind. From this relation, we presume that regulation of accretion is mainly conducted by winds for $a_{sBH} \lesssim [f_w/(\dot{m}_{sBH}\eta_{rad})]^{1/2}$, although understanding this transition in detail would require performing hydrodynamical simulations. We conclude that the effect of the wind on the cocoon evolution can be neglected for a rapidly accreting and spinning sBH.

B.3. Regulation of Accretion by Winds/Outflows

In this section, we evaluate regulation of accretion onto the sBH by radiation-driven winds (outflows) launched from a rapidly accreting CsBD. Figure 7 shows various properties of the shock produced by the wind. The wind density without interactions is given by $\rho_w = \frac{\dot{M}_w}{\Omega_w \beta_w c z^2}$, which is lower than the disk density at the scale height of the AGN disk (blue line in Figure 7(b)). This suggests that the wind is decelerated before breakout from the AGN disk. When radiation is inefficient, the internal pressure of the shocked fluid is dominated by the thermal energy ($P_{ad,w} = k_B T_{ad} n_{AGN}$; black in panel (b)), where $T_{ad} = 0.7 L_w t_{break,w}/(3/2 k_B n_{AGN} V_{sh,w})$ is the proton temperature at breakout assuming negligible radiative cooling (e.g., McKee & Ostriker 1977; orange line in panel (c)), $L_w = \dot{M}_w v_w^2$ is the wind luminosity, $t_{break,w} = H_{AGN}/v_{ad,w}$ is the breakout timescale of the wind shock from the AGN disk assuming adiabatic evolution (solid black in panel (c)), $v_{ad,w}$ is the shock velocity at breakout assuming adiabatic evolution, and $V_{sh,w}$ is the volume of the shocked region at the breakout.

When the photon diffusion velocity from the AGN disk (c/τ) exceeds the velocity of the wind shock ($v_{sh,w}$), photons can escape from each shocked shell, where $\tau = 2\rho_{AGN}H_{AGN}\kappa_{AGN}$ is the optical depth of the AGN disk. Since $v_{ad,w}$ is the upper limit for $v_{sh,w}$, the diffusion of photons is faster than the shock velocity

$(v_{\mathrm{sh},w} \lesssim v_{\mathrm{ad},w} < c/\tau$; solid and dashed orange lines in Figure 7(b)). Then, the energy-loss rate by cooling may reduce the internal pressure of the shocked regions. The cooling of protons becomes efficient when $t_{\mathrm{break},w}$ is shorter than the Coulomb loss timescale $(t_{\mathrm{Coulomb}} = m_p m_e c_{s,\mathrm{ad}}^3 3^{3/2}/(8\pi e^4 n_{\mathrm{AGN}} \log\Lambda)$; e.g., Dermer & Menon 2009; dashed black in panel (c)), where m_p and m_e are the proton and electron masses, respectively, $\log\Lambda = \log(r_{\mathrm{D}}/r_c)$ is the Coulomb logarithm, r_{D} is the Debye length, $r_c = e^2/k_{\mathrm{B}}T_{\mathrm{ad}}$ is the collision parameter, e is the elementary charge, and $c_{s,\mathrm{ad}}$ is the sound speed of protons with the temperature T_{ad}. In the fiducial model, $t_{\mathrm{break},w}$ exceeds t_{Coulomb} at $0.1\,\mathrm{pc} \gtrsim R \gtrsim 0.003\,\mathrm{pc}$ and $R \sim 3 \times 10^{-4}\,\mathrm{pc}$. In these regions, cooling of protons and loss of the shock energy (and reduction of the internal pressure) are expected to become efficient, since the Coulomb interaction converts the thermal energy of protons to that of electrons, and free–free emission converts the thermal energy of electrons to the radiation energy, with Compton scattering contributing at $R \lesssim 10^{-2}$–$10^{-3}\,\mathrm{pc}$, where the electron temperature and the Compton parameter (e.g., Rybicki & Lightman 1979) are presumed to be high. However, detailed analyses of the cooling processes require modeling the evolution of electrons considering interactions of a collisionless plasma, which are complicated and uncertain, and also cooling has a minor influence on the reduction of accretion as discussed below. For simplicity, we leave a more detailed analysis of cooling to a future study.

If the shocked fluid is adiabatic, the internal energy of the shock produced by the wind is not negligible compared to the cocoon's internal energy (black line in panel (b)). This is because even though the luminosity of the wind is lower than that of the jet by a factor of $\sim c^2/v_w^2$ assuming the same conversion efficiency ($\eta_j \sim \dot{M}_w/\dot{M}_{\mathrm{sBH}}$), there is a long time for the wind to deposit energy. $P_{\mathrm{ad},w}$ is lower than P_c mostly because the volume of the wind shock is larger than that of the cocoon by $\sim\theta_0^{-2}$. Note that the dependence of t_{cons} and t_{re} on θ_0 is roughly the same, so θ_0 does not contribute to the reduction rate. By performing a similar analysis to the JFM using $P_{\mathrm{ad},w}$ (solid black in panel (b)), we can estimate the reduction rate of accretion onto the sBH by the wind assuming adiabatic evolution of the wind shock (solid black line in panel (a) of Figure 7). By comparing this reduction to that by the cocoon (orange line), we can see that the reduction rate of accretion onto the sBH by the wind is a minor contribution inside $R \lesssim 10^{-1}\,\mathrm{pc}$, while it can become comparable to that by the cocoon at $R \gtrsim 10^{-1}\,\mathrm{pc}$ if cooling is inefficient. As discussed above, the internal pressure of the wind shock can be reduced by cooling within $R \lesssim 0.1\,\mathrm{pc}$, while that at $R \gtrsim 10^{-1}\,\mathrm{pc}$ is less influenced. Thus, the reduction rate of accretion by the wind is roughly given by the black line in Figure 7(a). When the sBH is rapidly spinning and produces a strong BZ jet, the jet and the cocoon propagate faster and the JFM dominates as discussed in the previous section. On the other hand, for an sBH that is not rapidly spinning, the wind can play a dominant role in regulating accretion at $R \gtrsim 10^{-1}\,\mathrm{pc}$. If accretion of sBHs is mainly regulated by the wind shock, the critical radius for the ejection of captured gas is larger by a factor of $\sim P_c/P_{\mathrm{ad},w}$ (black line in Fig 7(b)) compared to that by the cocoon, due to less efficient heating by the winds. Then, the depletion of gas is not expected even for less massive SMBHs of $M_{\mathrm{SMBH}} \sim 10^4$–$10^5\,M_\odot$, which is different from the JFM (Section 4). Thus, quasar observations for less massive SMBHs with high accretion rates (Greene & Ho 2007) can be used to distinguish the feedback processes for accretion onto sBHs in these environments.

B.4. Influence of the Cocoon on Migration and Gasdynamical Friction

We next discuss the influence of the JFM on migration (e.g., Ostriker 1999). The migration of sBHs in an AGN disk is caused by resonant Lindblad and corotation torques (e.g., Armitage 2007), which are mainly contributed by gas outside and inside the Hill radius, respectively. As $r_{\mathrm{dep}} < H_{\mathrm{AGN}} \lesssim r_{\mathrm{Hill}}$, the corotation torque is predicted to be significantly affected, while the Lindblad torque is not. To understand how the corotational torque is modified, hydrodynamical simulations need to be performed.

We also investigate whether the depth of the gap is influenced by the cocoon evolution. Since the cocoon can eject gas that is captured by the sBH, the maximum ejection rate is this capture rate. We confirmed that the gas capture does not influence the gap-opening timescale and the gap depth in the fiducial cases since the gravitational torque from sBHs more efficiently opens the gap compared to the gas capture. The gravitational torque from an sBH is $T_{\mathrm{sBH}} \sim (M_{\mathrm{sBH}}/M_{\mathrm{SMBH}})^2(R_{\mathrm{sBH}}/H_{\mathrm{AGN}})^3 R_{\mathrm{sBH}}^4 \Omega_{\mathrm{Kep}}^2 \Sigma_{\mathrm{AGN}}$ (Kanagawa et al. 2018), where Σ_{AGN} is the surface density of the AGN disk, and the angular momentum of gas within the annular gap is $\Delta J \sim 2\pi R_{\mathrm{sBH}}^2 \Delta_{\mathrm{gap}} \Omega_{\mathrm{Kep}} \Sigma_{\mathrm{AGN}}$, where Δ_{gap} is the gap width. By comparing the timescale of gap opening by the gravitational torque ($t_{\mathrm{torque}} \sim \Delta J/T_{\mathrm{sBH}}$) to that by gas capture ($t_{\mathrm{cap}} \sim M_{\mathrm{gap}}/\dot{M}_{\mathrm{cap}}$), where $M_{\mathrm{gap}} \sim 2\pi R_{\mathrm{sBH}} \Delta_{\mathrm{gap}} \Sigma_{\mathrm{AGN}}$ is the disk mass within a gap, we can see that the gravitational torque dominates when $(M_{\mathrm{sBH}}/M_{\mathrm{SMBH}})^2 \gtrsim (f_c/2)(H_{\mathrm{AGN}}/R_{\mathrm{sBH}})^3(\Delta_{\mathrm{gap}}/R_{\mathrm{sBH}})(R_w R_h/R_{\mathrm{sBH}}^2)$. By roughly assuming $\Delta_{\mathrm{gap}} \sim R_{\mathrm{Hill}} \sim H_{\mathrm{AGN}}$, the condition can be simplified to $M_{\mathrm{sBH}}/M_{\mathrm{SMBH}} \gtrsim (H_{\mathrm{AGN}}/R_{\mathrm{sBH}})^3$, which is usually satisfied unless M_{SMBH} and $H_{\mathrm{AGN}}/R_{\mathrm{sBH}}$ are high. In the cases in which the AGN disk is thick, a gap can be efficiently created owing to gas capture by sBHs instead of gravitational torques.

Similarly, we consider the influence of the JFM on gasdynamical friction (e.g., Ostriker 1999). Since gasdynamical friction arises from torques from gas around the Bondi–Hoyle–Lyttleton radius, and $r_{\mathrm{dep}} < H_{\mathrm{AGN}} \ll r_{\mathrm{BHL}}$ in the AGN disk, we conclude that gasdynamical friction is not significantly affected by the cocoon evolution, which ejects gas within r_{dep}.

Hence, the prescription for migration of sBHs (Equation (A11)) and the number of sBHs captured by an AGN disk (Figure 3) ignoring the JFM are presumably justified.

Appendix C
Parameter Dependence

Finally, we discuss the parameter dependence of the regulation of gas accretion.

C.1. Final Mass

We study how the evolution of the sBH mass depends on the model parameters. Figure 8 shows M_{sBH} (Equation (A9)) for various choices of parameters. We can see that $M_{\mathrm{sBH}}(R_{\mathrm{sBH}})$ is very parameter dependent. As $M_{\mathrm{sBH,ini}}$ or f_{acc} decreases, the average accretion rate onto the sBH is reduced (solid and dashed orange lines; Equation (17)), which lowers the final mass of the sBH. For low α_{CsBD} (solid blue), the surface
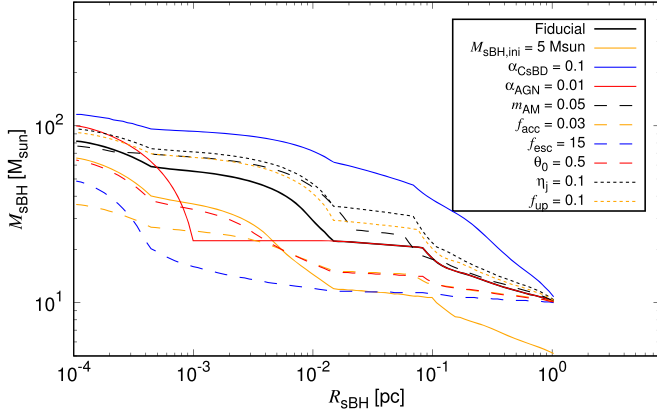
Figure 8. Same as in the bottom panel of Figure 5, but with parameters varied from the fiducial model as indicated in the legend.

Figure 9. Same as Figure 8, but for the total ejected mass from the AGN disk due to the JFM by the sBH migrating to R_{sBH}.

density of the CsBD is high, in which case the truncation radius is large, and the viscous timescale ($\sim t_{cons}$) at a fixed radius is long, both of which enhance the duty cycle (t_{cons}/t_{re}) and the growth rate of the sBH. A high value for f_{ext} or θ_0 increases r_{dep}, which reduces the duty cycle and the growth rate (dashed blue and red). When the angular momentum transfer parameter for the AGN disk is lower (solid red and dashed black), the surface density of the disk is higher, which enhances the accretion rate and the mass of the sBHs at a fixed location R_{sBH}. When the efficiency for producing the jet is weak (dotted black), the accretion becomes efficient as the ejected mass of the CsBD is reduced. We also investigate the case in which the gas density above the sBH is reduced to $\rho_{AGN}f_{up}$, possibly due to radiation and mechanical feedback. In this case, the pressure of the cocoon is reduced, and the regulation of accretion is weakened (dotted orange). Hence, the regulation of gas accretion by the cocoon strongly depends on many parameters (Equation (17)).

Figure 9 shows the total ejected mass from the AGN disk due to the JFM by the sBH migrating to R_{sBH}. We assume the ejected mass per one cocoon evolution to be $M_{eje} = \pi r_{dep}^2 H_{AGN} \rho_{AGN}$. From Figure 9, the ejected mass from the AGN disk is smaller than the accreted mass onto the sBH (Figure 3) except for the large f_{esc} and θ_0 cases (dashed blue and red lines), when gas in larger regions is ejected by the feedback. Even in such cases of efficient ejection, the ejected mass from the AGN disk does not contribute to the depletion of gas inflow.

C.2. Inclined Cases

In our modeling as described in the main text, we assume that the jet direction is the same as the angular momentum direction of the AGN disk. On the other hand, when the spin direction of the sBH is misaligned with respect to the angular momentum direction of the AGN disk (e.g., Schreier et al. 2019, for the inclined JFM in common envelope evolution), it takes a longer time for the jet and cocoon to break out. Then, the depletion region by the cocoon is effectively enhanced to $r_{dep} = f_{ext} H_{AGN} \theta_c / \cos i$, where i is the inclination angle of the jet with respect to the orbital angular momentum of the AGN disk.
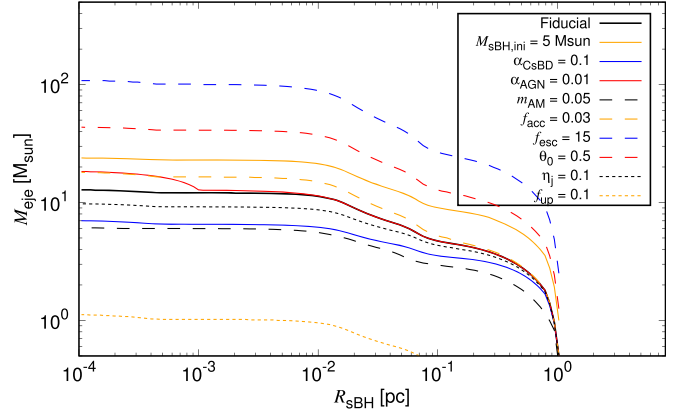
The sBH spins are often randomly oriented if enhanced by mergers in gap-forming regions (Tagawa et al. 2020a, 2021a). In this case, the resupply timescale increases by a factor of a few on average, which effectively reduces the average accretion rate by a similar factor. On the other hand, if sBH spins evolve owing to mergers in migration traps (Bellovary et al. 2016; Yang et al. 2019, 2020) or gas accretion (e.g., Safarzadeh & Haiman 2020) in the AGN disk, i is presumably close to zero, and the formulae for the depletion radius (Equation (12)) and the resupply timescale (Equation (14)) do not need revisions.

When the inclination exceeds $\pi/4$, the jet likely collides with thick regions of the CsBD within the trapping radius. In this case, geometrically thick inner regions are thermalized as a cocoon and ejected from the sBH. This cocoon possibly escapes without ejecting thin regions of the CsBD since shocked materials tend to proceed toward low-pressure regions (Kompaneets 1960). The overall picture of sBH growth should not be significantly modified in such cases. Since the probability is low (of about the aspect ratio of the disk), we ignore the situations in which the jet collides with geometrically thin regions of the CsBD, in which case most of the CsBD is probably ejected.

Meanwhile, if sBHs are formed in situ (Fahrion et al. 2021), their formation may be accompanied by long gamma-ray bursts (Zhu et al. 2021c; Perna et al. 2021a; Jermyn et al. 2021), supernova explosions (Grishin et al. 2021; Zhu et al. 2021a), or energetic transients associated with the accretion-induced collapse of neutron stars and white dwarfs (McKernan et al. 2020; Perna et al. 2021b; Zhu et al. 2021b). Thus, the first episode for gas ejection may be distinct from the later episodes. The observational signatures related to a jet and a cocoon will be investigated in a forthcoming paper.

Appendix D
Variables

D.1. Parameter Set

The fiducial model parameters are listed in Table 1.

D.2. Notation

The notations of variables are listed in Tables 2 and 3.

Table 2
Notation

Symbol	Description	Symbol	Description
r, z, R, Z	The cylindrical coordinates (z, r) and (Z, R) with $z = r = 0$ and $Z = R = 0$ as the positions of the sBH and the SMBH, respectively	R_{sBH}	The radial position of the sBH from the SMBH
$r_{\mathrm{BHL}}, r_{\mathrm{Hill}}$	The Bondi–Hoyle–Lyttleton radius and the Hill radius	$r_w = \min(r_{\mathrm{BHL}}, r_{\mathrm{Hill}})$, $r_h = \min(r_w, H_{\mathrm{AGN}})$	The capture radius and height of gas by an sBH
$r_{\mathrm{tru}}, r_{\mathrm{dep}}, r_c$	The truncation radius outside which the CsBD is truncated, the depletion radius within which the AGN gas is ejected, and the r-direction extent of the cocoon at the jet breakout	$r_{\mathrm{CsBD,out}}, r_{\mathrm{vis}}$	The outer radius of the CsBD, and the radial distance from the sBH at which the viscous timescale becomes equal to the resupply timescale (t_{re})
H_{AGN}	The scale height of the AGN disk	z_{eq}	The equilibrium height at which the pressures by the cocoon and the wind become equal
$v_{\mathrm{CsBD,Kep}}(r)$	The Keplerian velocity of the CsBD at the distance r from the sBH	Ω_{Kep}	The Keplerian angular velocity around the SMBH
$c_{s,\mathrm{AGN}}, v_{\mathrm{sBH}}, v_{\mathrm{sh}}$	The sound velocity of the AGN disk, the velocity of the sBH with respect to the local AGN motion, and the shear velocity at the capture radius (r_w)	$v_w = \beta_w c, \dot{M}_w, \Omega_w$	The velocity, outflow rate, and solid angle of the wind
$M_{\mathrm{sBH}}, M_{\mathrm{SMBH}}$	The mass of the sBH and the SMBH	$M_{\mathrm{sBH,ini}}, M_{\mathrm{sBH,fin}}$	The mass of the sBH at $t = 0$ and $t = t_{\mathrm{AGN}}$
$M_{\mathrm{annu}}, M_{\mathrm{ej}}$	The gas mass within annulus with the width of r_{Hill} around the sBH, and the ejection mass by the cocoon evolution	$M_{\mathrm{CsBD,tru}}$	The CsBD mass after the truncation (with the radius r_{tru}) by the evolution of the cocoon
$\dot{M}_{\mathrm{cap}}, \dot{M}_{\mathrm{in,vis}}, \dot{M}_{\mathrm{sBH}}$	The capture rate (Equation (1)), the inflow rate within r_{vis}, and the accretion rate onto an sBH	$\dot{M}_{\mathrm{Edd}}(M)$	The Eddington accretion rate onto a BH with the mass M
$\dot{M}_{\mathrm{sBH,tot}}$	The depletion rate by all sBHs embedded in an AGN disk	$\dot{M}_{\mathrm{CsBD,Kep}}(<r)$	The cumulative mass accretion rate of accreting gas after redistributing the radial distances r where their specific angular momentum matches that of the local Keplerian rotation
$\dot{m}_{\mathrm{SMBH}} = \dot{M}_{\mathrm{SMBH,in}}/\dot{M}_{\mathrm{Edd}}$	The gas inflow rate from the outer boundary of the AGN disk in units of the Eddington rate for M_{SMBH}	$\dot{M}_{\mathrm{SMBH,in}}$	The inflow rate of the AGN disk from the outer boundary (R_{out})
Σ_{CsBD}	The surface density of the CsBD	$\Sigma_{\mathrm{disk}}, \Sigma_{\mathrm{disk,min}}$	The surface density of the AGN disk and that after a gap forms
$\rho_{\mathrm{AGN}}, \Sigma_{\mathrm{AGN}}$	The density and surface density of the AGN disk	$L_{\mathrm{Edd}}(M), \eta_{\mathrm{rad}}$	The Eddington luminosity for the mass M, and the conversion efficiency to radiation
$f_{\mathrm{acc}} = \dot{M}_{\mathrm{sBH}}/\dot{M}_{\mathrm{cap}}$	The reduction factor of the captured gas	$f_{\mathrm{acc,eff}} = \dot{M}_{\mathrm{sBH,ave}}/\dot{M}_{\mathrm{cap}}$	The averaged reduction factor of the captured gas
f_{circ}	The ratio of the outer radius of the CsBD over the Hill radius	$f_{\mathrm{ext}} = r_{\mathrm{dep}}/r_c$	The fraction that the cocoon proceeds to the r-direction after the breakout
$f_w = \dot{M}_w/\dot{M}_{\mathrm{cap}}$	The fraction of the wind-loss rate over the capture rate	$N_{\mathrm{AGN,sBH}}$	The typical number of sBHs embedded in an AGN disk
$t_{\mathrm{re}}, t_{\mathrm{cons}}$	The resupply timescale of ejected gas ejected by the cocoon evolution, and the consumption timescale of the bound CsBD after the cocoon evolution	$t_{\mathrm{I}}, t_{\mathrm{I,II}}$	The type I and type I/II migration timescale
t_{break}	The breakout timescale of the cocoon	$t_{\mathrm{gap,ej}}$	The timescale of the gas ejection of the mass, M_{annu}
t_{AGN}	The typical total AGN phases in a galaxy	t_{mig}	The migration timescale in disks
$\tilde{L}$	The ratio between the energy density of the jet and the rest-mass energy density of the AGN disk	L_j, η_j	The luminosity of the jet, and the conversion efficiency to the jet
$\beta_h, \beta_c, \Gamma_j$	The head velocity and the lateral expansion velocity of the cocoon, and the Lorentz factor just below the head	E_c, V_c, P_c	The energy, volume, and pressure of the cocoon
θ_0, θ_c	The opening angle of injected jet and the cocoon	a_{sBH}	The dimensionless spin of the sBH
$\alpha_{\mathrm{CsBD}}, \alpha_{\mathrm{AGN}}$	The viscous parameter for the CsBD and the AGN disk	m_{AM}	The angular momentum transfer parameter for outer regions of the AGN disk
$\kappa_{\mathrm{CsBD}}, \kappa_{\mathrm{AGN}}$	The opacity of the CsBD and the AGN disk	K	The parameter representing the depth of a gap

Table 3
Notation

Symbol	Description	Symbol	Description
c	The speed of light	k_B	The Boltzmann constant
v_{esc}	The escape velocity from the SMBH	i	The inclination angle between the jet and the orbital angular momentum of the AGN disk
ν	The viscosity	$\alpha_{eff} = \nu/(c_{s,AGN}H_{AGN})$	The effective α parameter
ρ_w	The wind density	L_w	The wind luminosity
$v_{sh,w}$, $v_{ad,w}$	The shock velocity, and that assuming the adiabatic evolution at breakout from the AGN disk	T_{ad}	The gas temperature for the shocked fluid at breakout from the AGN disk assuming adiabatic evolution
P_{ad}	The thermal pressure with the temperature T_{ad}	$V_{sh,w}$	The volume of the shocked region at breakout from the AGN disk
$t_{break,w}$	The breakout timescale from the AGN disk of the wind shock assuming adiabatic evolution	$t_{Coulomb}$	The Coulomb loss timescale
t_{acc}	The accretion timescale	M_{crit}	The critical mass for the sBH at which $t_{acc} = t_I$
m_p, m_e	The proton and electron masses	$\log(\Lambda)$	The Coulomb logarithm
r_D, r_c	The Debye length and the collision length	e	The elementary charge
$\tau = 2\rho_{AGN}H_{AGN}\kappa_{AGN}$	The optical depth of the AGN disk	y_{comp}	The Compton parameter

ORCID iDs

Shigeo S. Kimura ● https://orcid.org/0000-0003-2579-7266
Zoltán Haiman ● https://orcid.org/0000-0003-3633-5403
Rosalba Perna ● https://orcid.org/0000-0002-3635-5677
Hidekazu Tanaka ● https://orcid.org/0000-0001-9659-658X
Imre Bartos ● https://orcid.org/0000-0001-5607-3637

References

Abbott, R., Abbott, T. D., Abraham, S., et al. 2020, PhRvL, 125, 101102
Abramowicz, M. A., Czerny, B., Lasota, J. P., & Szuszkiewicz, E. 1988, ApJ, 332, 646
Armitage, P. J. 2007, arXiv:astro-ph/0701485
Artymowicz, P., Lin, D. N. C., & Wampler, E. J. 1993, ApJ, 409, 592
Ayliffe, B. A., & Bate, M. R. 2009, MNRAS, 397, 657
Balick, B., & Frank, A. 2002, ARA&A, 40, 439
Baruteau, C., Cuadra, J., & Lin, D. N. C. 2011, ApJ, 726, 28
Barvainis, R. 1987, ApJ, 320, 537
Belczynski, K., Bulik, T., Fryer, C., et al. 2010, ApJ, 714, 1217
Bell, K. R., & Lin, D. N. C. 1994, ApJ, 427, 987
Bellovary, J. M., Mac Low, M. M., McKernan, B., & Ford, K. E. S. 2016, ApJL, 819, L17
Berger, E. 2014, ARA&A, 52, 43
Blandford, R. D., & Begelman, M. C. 1999, MNRAS, 303, L1
Blandford, R. D., & Znajek, R. L. 1977, MNRAS, 179, 433
Bromberg, O., Granot, J., Lyubarsky, Y., & Piran, T. 2014, MNRAS, 443, 1532
Bromberg, O., Nakar, E., Piran, T., & Sari, R. 2011, ApJ, 740, 100
Buonanno, A., Kidder, L. E., & Lehner, L. 2008, PhRvD, 77, 026004
Burtscher, L., Meisenheimer, K., Tristram, K. R. W., et al. 2013, A&A, 558, 149
Cantiello, M., Jermyn, A. S., & Lin, D. N. C. 2021, ApJ, 910, 94
Cao, X. 2011, ApJ, 737, 94
Chamandy, L., Frank, A., Blackman, E. G., et al. 2018, MNRAS, 480, 1898
Chen, W.-X., & Beloborodov, A. M. 2007, ApJ, 657, 383
Dermer, C. D., & Menon, G. 2009, High Energy Radiation from Black Holes: Gamma Rays, Cosmic Rays, and Neutrinos (Princeton, NJ: Princeton Univ. Press)
Di Matteo, T., Perna, R., & Narayan, R. 2002, ApJ, 579, 706
Dittmann, A. J., Cantiello, M., & Jermyn, A. S. 2021, ApJ, 916, 48
Do, T., Kerzendorf, W., Konopacky, Q., et al. 2018, ApJL, 855, L5
Duffell, P. C., Haiman, Z., MacFadyen, A. I., D'Orazio, D. J., & Farris, B. D. 2014, ApJL, 792, L10
Fabian, A. C. 2012, ARA&A, 50, 455
Fahrion, K., Lyubenova, M., van de Ven, G., et al. 2021, A&A, 650, A137
Frank, A., Ray, T. P., Cabrit, S., et al. 2014, in Protostars and Planets VI, ed. H. Beuther et al. (Tucson, AZ: Univ. Arizona Press)
Fung, J., Shi, J. M., & Chiang, E. 2014, ApJ, 782, 88
Goodman, J. 2003, MNRAS, 339, 937
Goodman, J., & Tan, J. C. 2004, ApJ, 608, 108

Graham, M. J., Ford, K. E. S., McKernan, B., et al. 2020, PhRvL, 124, 251102
Gravity Collaboration, Abuter, R., Amorim, A., et al. 2020, A&A, 636, L5
Greene, J. E., & Ho, L. C. 2007, ApJ, 667, 131
Grichener, A., Cohen, C., & Soker, N. 2021, ApJ, 922, 61
Grishin, E., Bobrick, A., Hirai, R., Mandel, I., & Perets, H. B. 2021, MNRAS, 507, 156
Gruzinov, A., Levin, Y., & Matzner, C. D. 2020, MNRAS, 492, 2755
Hada, K., Doi, A., Wajima, K., et al. 2018, ApJ, 860, 141
Hada, K., Kino, M., Doi, A., et al. 2013, ApJ, 775, 70
Hailey, C. J., Mori, K., Bauer, F. E., et al. 2018, Nature Letter, 556, 70
Haiman, Z., Kocsis, B., & Menou, K. 2009, ApJ, 700, 1952
Hillel, S., Schreier, R., & Soker, N. 2021, arXiv:2112.01459
Inayoshi, K., Haiman, Z., & Ostriker, J. P. 2016, MNRAS, 459, 3738
Janiuk, A., Perna, R., Di Matteo, T., & Czerny, B. 2004, MNRAS, 355, 950
Jermyn, A. S., Dittmann, A. J., Cantiello, M., & Perna, R. 2021, ApJ, 914, 105
Jiang, Y.-F., Stone, J. M., & Davis, S. W. 2014, ApJ, 796, 106
Jiao, C.-L., Mineshige, S., Takeuchi, S., & Ohsuga, K. 2015, ApJ, 806, 93
Kanagawa, K. D., Muto, T., Tanaka, H., et al. 2015, ApJL, 806, L15
Kanagawa, K. D., Tanaka, H., & Szuszkiewicz, E. 2018, ApJ, 861, 140
Kashiyama, K., Nakauchi, D., Suwa, Y., Yajima, H., & Nakamura, T. 2013, ApJ, 770, 8
Kato, S., Fukue, J., & Mineshige, S. 2008, Black-Hole Accretion Disks – Towards a New Paradigm (Kyoto: Kyoto Univ. Press)
Kimura, S. S., Murase, K., & Bartos, I. 2021a, ApJ, 916, 111
Kimura, S. S., Sudoh, T., Kashiyama, K., & Kawanaka, N. 2021b, ApJ, 915, 31
King, A. R., Pringle, J. E., & Livio, M. 2007, MNRAS, 376, 1740
Kitaki, T., Mineshige, S., Ohsuga, K., & Kawashima, T. 2021, PASJ, 73, 450
Kohri, K., Narayan, R., & Piran, T. 2005, ApJ, 629, 341
Kompaneets, D. A. 1960, DoSSR, 130, 1001
Kormendy, J., & Ho, L. C. 2013, ARA&A, 51, 511
Kratter, K., & Lodato, G. 2016, ARA&A, 54, 271
Levin, Y. 2007, MNRAS, 374, 515
Levin, Y., & Beloborodov, A. M. 2003, ApJL, 590, L33
Li, X., Chang, P., Levin, Y., Matzner, C. D., & Armitage, P. J. 2020, MNRAS, 494, 2327
Liska, M., Tchekhovskoy, A., & Quataert, E. 2020, MNRAS, 494, 3656
López-Cámara, D., De Colle, F., & Moreno Méndez, E. 2019, MNRAS, 482, 3646
Lu, J. R., Do, T., Ghez, A. M., et al. 2013, ApJ, 764, 155
Lubow, S. H., Seibert, M., & Artymowicz, P. 1999, ApJ, 526, 1001
Marconi, A., Risaliti, G., Gilli, R., et al. 2004, MNRAS, 351, 169
Martin, R. G., & Lubow, S. H. 2011, MNRAS, 413, 1447
Martin, R. G., Nixon, C. J., Pringle, J. E., & Livio, M. 2019, NewA, 70, 7
McKee, C. F., & Ostriker, J. P. 1977, ApJ, 218, 148
McKernan, B., Ford, K. E. S., & O'Shaughnessy, R. 2020, MNRAS, 498, 4088
McNamara, B. R., & Nulsen, P. E. J. 2012, NJPh, 14, 055023
Meier, D. L. 2001, ApJL, 548, L9
Merritt, D. 2010, ApJ, 718, 739
Milosavljević, M., Bromm, V., Couch, S. M., & Oh, S. P. 2009, ApJ, 698, 766
Miralda-Escude, J., & Gould, A. 2000, ApJ, 545, 847
Moreno Méndez, E., López-Cámara, D., & De Colle, F. 2017, MNRAS, 470, 2929

Mori, K., Hailey, C. J., Schutt, T. Y. E., et al. 2021, ApJ, 921, 148
Naoz, S., Will, C. M., Ramirez-Ruiz, E., et al. 2020, ApJL, 888, L8
Narayan, R., Chael, A., Chatterjee, K., Ricarte, A., & Curd, B. 2021, MNRAS, in press
Narayan, R., & Yi, I. 1994, ApJL, 428, L13
Nayakshin, S., Cuadra, J., & Springel, V. 2007, MNRAS, 379, 21
Olano, C. A. 2009, A&A, 506, 1215
Ostriker, E. C. 1999, ApJ, 513, 252
Ostriker, J. P. 1983, ApJ, 273, 99
Paardekooper, S.-J., Baruteau, C., Crida, A., & Kley, W. 2010, MNRAS, 401, 1950
Pan, Z., & Yang, H. 2021, ApJ, 923, 173
Park, K., & Ricotti, M. 2011, ApJ, 739, 2
Park, K., & Ricotti, M. 2012, ApJ, 747, 9
Perna, R., Hernquist, L., & Narayan, R. 2000, ApJ, 541, 344
Perna, R., Lazzati, D., & Cantiello, M. 2021a, ApJL, 906, L7
Perna, R., Tagawa, H., Haiman, Z., & Bartos, I. 2021b, ApJ, 915, 10
Pushkarev, A. B., Kovalev, Y. Y., Lister, M. L., & Savolainen, T. 2009, A&A, 507, L33
Regan, J. A., Downes, T. P., Volonteri, M., et al. 2019, MNRAS, 486, 3892
Rosenthal, M. M., Chiang, E. I., Ginzburg, S., & Murray-Clay, R. A. 2020, MNRAS, 498, 2054
Rybicki, G. B., & Lightman, A. P. 1979, Radiative Processes in Astrophysics (New York: Wiley)
Sadowski, A., Narayan, R., Tchekhovskoy, A., et al. 2015, MNRAS, 447, 49
Safarzadeh, M., & Haiman, Z. 2020, ApJL, 903, L21
Samsing, J., Bartos, I., D'Orazio, D. J., et al. 2020, arXiv:2010.09765
Schödel, R., Nogueras-Lara, F., Gallego-Cano, E., et al. 2020, A&A, 641, A102
Schreier, R., Hillel, S., & Soker, N. 2019, MNRAS, 490, 4748
Shakura, N. I., & Sunyaev, R. A. 1973, A&A, 24, 337
Soker, N. 2014, arXiv:1404.5234
Soker, N. 2016, NewAR, 75, 1
Stalevski, M., Tristram, K. R. W., & Asmus, D. 2019, MNRAS, 484, 3334
Stone, N. C., Metzger, B. D., & Haiman, Z. 2017, MNRAS, 464, 946
Su, M., Slatyer, T. R., & Finkbeiner, D. P. 2010, ApJ, 724, 1044
Sugimura, K., Hosokawa, T., Yajima, H., & Omukai, K. 2017, MNRAS, 469, 62
Syer, D., Clarke, C. J., & Rees, M. J. 1991, MNRAS, 250, 505
Szolgyen, A., & Kocsis, B. 2018, PhRvL, 121, 101101
Szulágyi, J., Binkert, F., & Surville, C. 2022, ApJ, 924, 1
Tagawa, H., Haiman, Z., Bartos, I., & Kocsis, B. 2020a, ApJ, 899, 26
Tagawa, H., Haiman, Z., Bartos, I., Kocsis, B., & Omukai, K. 2021a, MNRAS, 507, 3362
Tagawa, H., Haiman, Z., & Kocsis, B. 2020b, ApJ, 898, 25
Tagawa, H., Kocsis, B., Haiman, Z., et al. 2021b, ApJL, 907, L20
Tagawa, H., Kocsis, B., Haiman, Z., et al. 2021c, ApJ, 908, 194
Takeo, E., Inayoshi, K., & Mineshige, S. 2020, MNRAS, 497, 302
Tanaka, H., Murase, K., & Tanigawa, T. 2020, ApJ, 891, 143
Tanaka, H., Takeuchi, T., & Ward, W. R. 2002, ApJ, 565, 1257
Tanigawa, T., Ohtsuki, K., & Machida, M. N. 2012, ApJ, 747, 47
Tanigawa, T., & Tanaka, H. 2016, ApJ, 823, 48
Tanigawa, T., & Watanabe, S.-i 2002, ApJ, 580, 506
Tchekhovskoy, A., Narayan, R., & McKinney, J. C. 2010, ApJ, 711, 50
Tchekhovskoy, A., Narayan, R., & McKinney, J. C. 2011, MNRAS, 418, L79
Thompson, T. A., Quataert, E., & Murray, N. 2005, ApJ, 630, 167
Toyouchi, D., Hosokawa, T., Sugimura, K., & Kuiper, R. 2020, MNRAS, 496, 1909
Toyouchi, D., Hosokawa, T., Sugimura, K., Nakatani, R., & Kuiper, R. 2019, MNRAS, 483, 2031
Toyouchi, D., Inayoshi, K., Hosokawa, T., & Kuiper, R. 2021, ApJ, 907, 74
Wagner, A. Y., & Bicknell, G. V. 2011, ApJ, 728, 29
Wang, J.-M., Liu, J.-R., Ho, L. C., & Du, P. 2021a, ApJL, 911, L14
Wang, J.-M., Liu, J.-R., Ho, L. C., Li, Y.-R., & Du, P. 2021b, ApJL, 916, L17
Ward, W. R. 1997, Icar, 126, 261
Xu, F., Bian, F., Shen, Y., et al. 2018, MNRAS, 480, 345
Yang, Y., Bartos, I., Gayathri, V., et al. 2019, PhRvL, 123, 181101
Yang, Y., Gayathri, V., Bartos, I., et al. 2020, ApJL, 901, L34
Yu, Q., & Tremaine, S. 2002, MNRAS, 335, 965
Zhu, J.-P., Wang, K., & Zhang, B. 2021a, ApJL, 917, L28
Zhu, J.-P., Yang, Y.-P., Zhang, B., et al. 2021b, ApJL, 914, L19
Zhu, J.-P., Zhang, B., Yu, Y.-W., & Gao, H. 2021c, ApJL, 906, L11